Cover Page

Universiteit Leiden

The handle http://hdl.handle.net/1887/58472 holds various files of this Leiden University dissertation.

Author: Witte, W.E.A. de
Title: Mechanistic modelling of drug target binding kinetics as determinant of the time course of drug action in vivo
Issue Date: 2017-12-19

Chapter 7. Modelling the delay between PK and EEG effects of morphine in rats; binding kinetic *versus* effect compartment models

Wilhelmus E.A. de Witte[1], Vivi Rottschäfer[2], Meindert Danhof[1], Piet H. van der Graaf[1,3], Lambertus A. Peletier[2], Elizabeth C.M. de Lange[1*].

[1] Division of Pharmacology, Leiden Academic Centre for Drug Research, Leiden University, 2333 CC Leiden, The Netherlands

[2] Mathematical Institute, Leiden University, 2333, CA Leiden, The Netherlands.

[3] Certara Quantitative Systems Pharmacology, Canterbury Innovation Centre, Canterbury CT2 7FG, United Kingdom

* Correspondence: ecmdelange@lacdr.leidenuniv.nl

Manuscript under revision for the Journal of Pharmacokinetics and Pharmacodynamics

Abstract

Introduction. Drug-target binding kinetics (as determined by association and dissociation rate constants, k_{on} and k_{off}) can be an important determinant of the kinetics of drug action. However, the effect compartment model is used most frequently instead of a target binding model to describe hysteresis. Here we investigate when the drug-target binding model should be used in lieu of the effect compartment model.

Methods. We tested the utility of the effect compartment (EC), the target binding kinetics (TB) and the combined effect compartment-target binding kinetics (EC-TB) model on either plasma (EC_{PL}, TB_{PL} and EC-TP_{PL}) or brain extracellular fluid (EC_{ECF}, TB_{ECF} and EC-TP_{ECF}) morphine concentrations and EEG amplitude in rats. We also analyzed when a significant shift in the time to maximal target occupancy ($Tmax_{TO}$) with increasing dose, the discriminating feature between the TB and EC model, occurs in the TB model. All TB models assumed a linear relationship between target occupancy and drug effect on the EEG amplitude.

Results. We found that all three model types performed similarly in describing the morphine PD data, although the EC model provided the best statistical result. Our analysis of the shift in $Tmax_{TO}$ ($\Delta Tmax_{TO}$) as a result of increasing dose revealed that $\Delta Tmax_{TO}$ is decreasing towards zero if the k_{off} is much smaller than the elimination rate constant or if the target concentration is larger than the initial morphine concentration.

Discussion and Conclusion. Our results for the morphine PKPD modelling and the analysis of $\Delta Tmax_{TO}$ indicate that the EC and TB models do not necessarily lead to different drug effect *versus* time curves for different doses if a delay between drug concentrations and drug effect (hysteresis) is described. Drawing mechanistic conclusions from successfully fitting one of these two models should therefore be avoided. Since the TB model can be informed by *in vitro* measurements of k_{on}, either plasma (a target binding model should be considered more often for mechanistic modelling purposes

Abbreviations: AIC: Akaike Information Criterion, CNS: Central Nervous System, DE: Direct Effect, ECF: Extracellular Fluid, EC: Effect Compartment, IE: Indirect Effect, GOF: Goodness Of Fits, IIV: Inter-Individual Variability, OFV: Objective Function Value, PD: Pharmacodynamics, Pgp: P-glycoprotein, PK: Pharmacokinetics, PD: Pharmacodynamics, TB: Target binding, $Tmax_{PD}$: Time between dosing and maximal drug effect, $Tmax_{TO}$: Time between dosing and maximal target occupancy, $\Delta Tmax_{TO}$: $Tmax_{TO}$ of the lower dose - $Tmax_{TO}$ of the higher dose, VPC: Visual Predictive Check

Introduction

Drug-target binding kinetics is an important criterion in the selection of drug candidates, as it can be a determinant of the time course and the selectivity of drug effect.[1–4]

However, the *in vivo* time course of drug action is influenced by multiple factors including plasma pharmacokinetics, target site distribution, target binding kinetics, competition with endogenous ligands, turnover of the target, signal transduction kinetics and the kinetics of homeostatic feedback. As a consequence, the influence of binding kinetics on drug action can only be understood in conjunction with these kinetic processes and its relevance is still not fully understood and subject to an ongoing debate.[3,5–8]

One of the arguments against an important role of binding kinetics for *in vivo* drug action is that binding kinetics are most often not required to get a good fitting PKPD model for small molecules. However, numerous examples are available were binding kinetic models have been successfully applied, and binding kinetics are routinely incorporated in models for biologics and PET data.[9–17] The sparsity of target binding PKPD models for small molecules can be explained by the relatively fast binding kinetics of many drugs currently on the market, compared to their pharmacokinetics.[3] In addition, when a delay between drug concentrations and effect is observed, this delay is often described by an effect compartment or indirect response model.[18,19]

Here we study the difference between the effect compartment (EC) model, the target binding (TB) model the direct effect (DE) and the indirect effect (IE) model which are described below. The EC model describes the delay between pharmacokinetics (PK) and pharmacodynamics (PD) by including first order distribution of the drug into and out of a hypothetical target-site (biophase) compartment, which drives the PD mostly in a nonlinear fashion.[20] The indirect effect (IE) model describes the delay between PK and PD by the zero order synthesis and first order degradation of an effector molecule which represents the PD, mostly in a linear fashion.[21] The target binding (TB) model describes the delay between PK and PD by the second order drug-target association and first order dissociation of the drug-target complex, which drives the effect in a linear or nonlinear fashion, depending on the efficacy and receptor reserve.[22–24] The DE model describes no delay between the PK and PD and links the drug concentration directly to the effect measurements in a linear or nonlinear fashion.

These models thus result in a zero, first and second order formation of the compounds that drives the PD, being the drug concentration in the effect compartment, the target-bound drug concentrations and the endogenous effector molecule in the EC, TB and IE model, respectively. This results in different dose dependencies of the time to the maximal effect $Tmax_{PD}$. As a current paradigm, the shift in $Tmax_{PD}$ ($\Delta Tmax_{PD}$) in a PKPD dataset as a consequence of a change in the dose, identifies the appropriate PKPD model to describe the data: with increasing dose, the $Tmax_{PD}$ can increase for the indirect response model, decrease for the TB model and is constant for the EC model.[25–27]

However, in contrast to common belief, the indirect response model does not always result in an increasing $Tmax_{PD}$ with increasing doses but can also give rise to a decreasing $Tmax_{PD}$ with increasing doses, as shown by Peletier et al.[28] A comprehensive analysis of the conditions for which a shift in $Tmax_{TO}$ for changing doses occurs in a TB model is currently not available. It might be that EC models have been used while TB models could have been applied equally well to describe the data in previous PKPD studies.

One example in which performance of TB and EC models has been investigated indicates comparable performance in describing the data of eight calcium channel blockers, but this study used only one dose level for all drugs[14] and therefore cannot be used to validate the relationship between dose and $\Delta Tmax_{PD}$. An additional complexity in choosing the most appropriate PKPD model to describe PKPD data is that, for most drugs, factors as target site distribution, drug-target binding and turnover of signaling molecules occur in parallel. It is not always needed to incorporate all these factors in the PKPD model, as only the rate limiting mechanism is required for a proper model fit that describes the observed data. However, leaving out such factors will never lead to understanding of the individual contributions and the interplay between

these factors. Combined EC-TB models[13,29,30] as well as combined IE-TB models[10] have been applied successfully to discriminate between the contributions of separate factors. However, this discrimination is not always possible if one of the factors is relatively fast and does not contribute significantly to the delay between PK and PD.[31–33]. In short, the relevance of drug-target binding kinetics cannot be excluded if one of the other models is successfully fitted to a dataset, and there is a need to generate more insight into the difference between the TB model and the EC model.

The aim of the current study is to investigate if the TB and EC model can give similar drug effect *versus* time curves and under what conditions this will occur. In this study, we used a historical PKPD dataset for morphine [34] to compare the goodness of fit for the TB model with the EC model and the combined EC-TB model in describing the time course of the EEG effect following administration of 3 different doses of morphine (4, 10 and 40 mg/kg). Both plasma and brain ECF drug concentrations were measured and tested in this study to be connected to the PD via an EC, TB or EC-TB model. Subsequently, a more general insight in the shift of $Tmax_{TO}$ for different dose levels in the drug-target binding model is obtained to identify for what parameter values the TB model can be discriminated from the EC model based on the $\Delta Tmax_{TO}$. To that end, we performed comprehensive simulations and mathematical model analysis for a wide range of drug-target association and dissociation rate constants, for various plasma elimination rate constants, target concentrations, and dose levels.

Methods

Pharmacokinetic and pharmacodynamic (PKPD) data of morphine in rats

All PK and PD data used in this study were obtained from the experiments described earlier.[35] In short: Morphine was intravenously administered to Male Wistar rats, during a 10-minute infusion, in 4 different dose groups: 0, 4, 10 or 40 mg/kg with 5, 29, 11 and 14 animals, respectively. The P-glycoprotein (Pgp) inhibitor GF120918 or vehicle was given as a continuous infusion. In the group of 29 animals that received 4 mg/kg morphine, 9 animals received GF120918, the other 20 animals received the vehicle. Furthermore, while plasma concentrations were measured in all animals, brain ECF concentrations were measured with microdialysis in 29 animals, of which 15 received 4 mg/kg, 0 received 10 mg/kg, 9 received 40 mg/kg and 5 received 0 mg/kg morphine.

For the modelling data set, all data entries without time recordings, without concentration data or with concentration data equal to 0 were removed from the dataset. The lower limit of quantification for morphine in plasma samples was 88 nM and 1.75 nM for morphine in ECF samples. The PD of morphine was measured as the amplitude in the δ frequency range (0.5-4.5 Hz) of the EEG, and recorded every minute. The EEG data were further averaged for every 3-minute interval to reduce the noise and decrease the model fitting time.

General model fitting methods

Data fitting was based on minimization of the Objective Function Value (OFV = – 2*log likelihood) as implemented in NONMEM 7.3.[36] To account for the number of parameters for the comparison of non-nested models, the Akaike Information Criterion (AIC) was calculated by adding two times the number of estimated parameters to the OFV.[37] Variability in the data was described by IIV (Inter Individual Variability: variability in parameter values between animals) and a residual error term. IIV was implemented assuming a log-normal distribution according to equation 1:

$$P_i = P_{pop} * e^{\eta_i} \quad (1)$$

In which P_i is the individual parameter value, P_{pop} is the typical parameter value in the population and η_i is normally distributed around a mean of zero with variance ω^2 according to equation 2:

$$\eta_i \sim N(0, \omega^2) \quad (2)$$

The remaining variation between the data and the model predictions are incorporated as residual error for which both a proportional (equation 3) and a combined proportional and additive (equation 4) error model were tested.

$$obs_{ij} = pred_{ij} * (1 + \varepsilon_{prop,ij}) \quad (3)$$

$$obs_{ij} = pred_{ij} * (1 + \varepsilon_{prop,ij}) + \varepsilon_{add,ij} \quad (4)$$

In these equations, obs_{ij} is the observation, $pred_{ij}$ is the model prediction, $\varepsilon_{prop,ij}$ is the proportional error and $\varepsilon_{add,ij}$ is the additive error for individual *i* at time point *j*. Both $\varepsilon_{prop,ij}$ and $\varepsilon_{add,ij}$ are normally distributed around a mean of zero with variance σ^2 according to equation 5 and 6:

$$\varepsilon_{prop,ij} \sim N(0, \sigma^2) \quad (5)$$

$$\varepsilon_{add,ij} \sim N(0, \sigma^2) \quad (6)$$

Morphine plasma PK modelling

One-compartment, two-compartment and three-compartment models were fitted to the plasma PK data, with both proportional and additive plus proportional error models, and with IIV on the various parameters. The best fits (based on AICs) of each structural model were compared for their GOFs (Goodness Of Fits) and AICs. Since the purpose of the plasma PK modelling was to get the best possible input for the PD modelling, GOF was assessed by the AIC and by individual fits. Over- or underestimation of IIV and population parameter estimates and high uncertainties in population parameter estimates were not regarded as problematic, since only the right individual parameter estimates were required for PD modeling.

Morphine brain ECF PK Modelling

The individual parameter estimates that were estimated to describe the plasma PK were used as fixed parameters to describe the plasma PK profile as input for the brain ECF concentrations. To describe the ECF concentrations, we thus assumed that the distribution of the drug into and out of the ECF did not lead to a change in plasma concentrations. The best fits, based on the AICs, of each structural model were compared for their GOFs (Goodness Of Fits) and AICs. Since the purpose of the brain ECF PK modelling was to get the best possible input for the PD modelling, GOF was assessed by the AIC and by individual fits. Over- or underestimation of IIV and population parameter estimates and high uncertainties in population parameter estimates were not regarded as problematic, since only the right individual parameter estimates were required for PD modeling.

EEG PD modelling

To maximize the identifiability of the PD model parameters, all pharmacokinetic parameters were used as fixed parameters to describe the plasma and brain ECF concentrations as input for all the described PD models to describe EEG effects.[38] The different type of models that were tested are outlined in Table 1. For each model, the most informative variations on the model structure are given in the results section.

Table 1. Overview of the different model types, the data that were used and the model numbers as used in this manuscript. EC = Effect compartment, TB = target binding, EC-TB = effect compartment – target binding. IE = indirect effect, DE = direct effect and ECF = brain extracellular fluid.

Model type	Concentrations linked to effect	Model number
EC	PLasma	$EC_{PL}1 – EC_{PL}4$
EC	ECF	$EC_{ECF}1$
TB	PLasma	$TB_{PL}1 – TB_{PL}5$
TB	ECF	$TB_{ECF}1$
EC-TB	PLasma	$ECTB_{PL}1 – ECTB_{PL}5$
IE	ECF	$IE_{ECF}1$
DE	ECF	$DE_{ECF}1$

To compare structural models that linked plasma or brain ECF concentrations directly to the PD, the models that used plasma PK were fitted to the reduced dataset that only contained animals with plasma PK, brain ECF and EEG measurements. Model comparison was based on the AIC, visual inspection of the GOF and a VPC (Visual Predictive Check) to check if the IIV was captured appropriately.

Drug-target binding model simulations

Simulations with a one-compartment binding model with IV administration were performed for a wide range of k_{on} and k_{off} values and for a variety of elimination rate constants, target concentrations and drug dose levels. The $Tmax_{TO}$ was compared for 2 different doses to determine the influence of the drug dose on the $Tmax_{TO}$. The $\Delta Tmax_{TO}$ values were calculated by subtracting the $Tmax_{TO}$ of the highest dose from the $Tmax_{TO}$ of the lowest dose and $\Delta Tmax_{TO}$ was plotted against k_{on} and k_{off}.

Results

Morphine PK modelling

Modelling of morphine pharmacokinetic data in plasma and brain ECF as described in Supplement S 1 identified very similar model structures as previously described for pharmacokinetic modelling of the same dataset by Groenendaal and coworkers.[35] In short, the plasma concentrations were described by a 3-compartment model and the ECF concentrations were described by passive distribution into and out of the brain combined with saturable active influx and first-order efflux.

EEG PD modelling

EC_{PL} model fitting

EC and TB models have been applied to the morphine data to describe the relationship between the observed plasma concentrations and EEG amplitude and direct effect (DE) indirect effect (IE), EC and TB models have been applied to brain ECF and EEG amplitude data. The differential equations for these models are given in Supplement S 1. Firstly, the originally published EC_{PL} model structure was optimized by adding a slope parameter which describes the linear decline of EEG amplitude over time during the experiment independent of the drug effect, and including IIV on the baseline EEG amplitude only. For this model, a transit compartment was required between the plasma and the effect compartment.[34] An overview of the different variations on this basic model structure is given in Table 2. The structure of all EC_{PL} is identical and is depicted in Figure 1. Based on the AIC, the parameter estimates and the GOF, model $EC_{PL}1$ was chosen as the best parameterization for the effect compartment model in Figure 1.

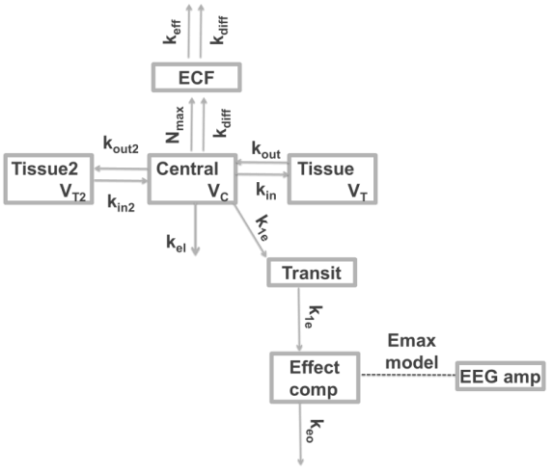

Figure 1. Schematic representation of the EC_{PL} model structure that was used to describe the morphine EEG amplitudes over time. k_{ie} = first-order in- and outward distribution rate constant for the transit compartment. k_{eo} first-order outward distribution rate constant from the effect compartment. The effect compartment concentrations were linked to the EEG amplitude by a sigmoidal Emax model. The distribution from plasma to the tissue compartments and the brain ECF compartment is described in Supplement S 1. The arrows indicate morphine flows, the dotted line indicates a direct relationship.

Table 2. Parameter values and objective function values of the tested EC models describing the EEG data based on plasma concentrations. CV denotes the coefficient of variation as percentage. OFV denotes the Objective Function Value, AIC denotes the Akaike Information Criterion. ω^2 and σ^2 denote the variances of the exponential IIV distribution and the error distribution, respectively.

	$EC_{PL}1$ selected model	**$EC_{PL}2$ no slope**	**$EC_{PL}3$ $k_{1e} = k_{eo}$**	**$EC_{PL}4$ no Pgp effect**
OFV	44748.0	45084.2	44853.3	44868.4
AIC	44770.0	45104.2	44871.3	44886.4
parameter	**Value (%CV)**	**Value (%CV)**	**Value (%CV)**	**Value (%CV)**
k_{1e}(/min)	0.0393 (18)	0.0432 (10)	0.0403 (10)	0.0375 (8)
k_{eo}(/min)	0.0382 (14)	0.0458 (9)	-	0.0375 (8)
k_{1e} -Pgp (/min)	0.0565 (44)	0.0661 (38)	0.0295 (18)	-
k_{eo} -Pgp (/min)	0.016 (46)	0.0203 (20)	-	-
E_0 (µV)	45.1 (4)	42.2 (4)	45.8 (4)	45.9 (4)
E_{max} (µV)	27.9 (23)	25.3 (16)	26.1 (18)	27.0 (18)
EC_{50} (nM)	1270 (52)	1220 (31)	912 (37)	1000 (37)
N_H	1.44 (43)	2.02 (27)	1.46 (36)	1.37 (33)
slope (µV/min)	-0.024 (22)	0 FIX	-0.0263 (15)	-0.0267 (15)
ω^2 E_0 (µV)	0.111 (20)	0.125 (19)	0.115 (20)	0.116 (20)
σ^2 proportional	0.0554 (7)	0.0584 (7)	0.0562 (6)	0.0564 (6)

TB_{PL} model fitting

The TB_{PL} model was applied to describe target binding from plasma, all TB_{PL} models in Table 3 shared the same structure as represented in Figure 2. The parameter estimation results are given in Table 3. Since the target concentration is of influence only if it is similar to the drug concentration (which is mostly above 100 nM in plasma and in brain ECF, as shown in Supplement S 1), the target concentration could not be estimated in this model and was fixed to an arbitrary low value of 1 nM in the model

estimations. This low target concentration prevents the influence of the target concentration on the EEG amplitude in the model. The influence of blocking Pgp has been incorporated by estimating separate parameter values with and without the presence of Pgp blocker. While the influence of blocking Pgp on the k_{off} or K_D is mechanistically not plausible, the improved model fits for the models which incorporate these influences might indicate that the estimated k_{off} and K_D values refer to apparent values which include not only the molecular properties. The target occupancy is linearly related to the EEG amplitude in model $TB_{PL}1$ - $TB_{PL}5$, as nonlinear relationships could not be identified accurately in this study. On basis of the objective function values, model $TB_{PL}4$ was selected as the best drug-target binding model. It should be noted that the AIC of model $TB_{PL}4$ is 338 points higher than model $EC_{PL}1$, which means that model $EC_{PL}1$ performs better in fitting the data. All TB_{PL} models have one compartment less than the transit-EC models $EC_{PL}1$ - $EC_{PL}4$. Therefore, the combined EC-TB_{PL} models EC-$TB_{PL}1$ - EC-$TB_{PL}5$ were developed.

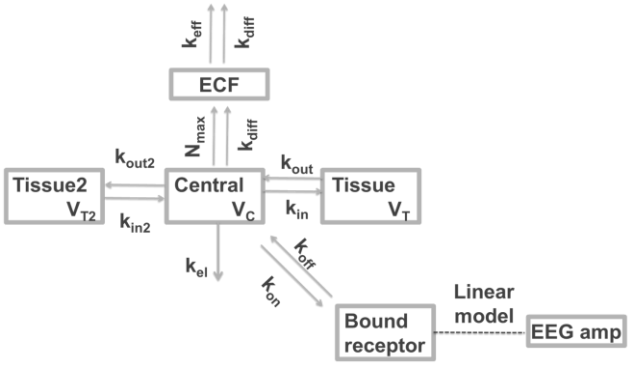

Figure 2. Schematic representation of the TB_{PL} model structure that was used to describe the morphine EEG amplitudes over time. k_{on} is the second-order drug-target association rate constant. k_{off} is the first-order drug-target dissociation rate constant. Target occupancy is linearly related to the EEG amplitude. The distribution from plasma to the tissue compartments and the brain ECF compartment is described in Supplement S 1. The arrows indicate morphine flows, the dotted line indicates a direct relationship.

Table 3. Parameter values and objective function values of the tested TB_{PL} models describing the EEG data based on plasma concentrations. CV denotes the coefficient of variation as percentage. OFV denotes the Objective Function Value, AIC denotes the Akaike Information Criterion. ω^2 and σ^2 denote the variances of the exponential IIV distribution and the error distribution, respectively.

	$TB_{PL}1$ no Pgp effect slope = 0	**$TB_{PL}2$ no Pgp effect**	**$TB_{PL}3$ Pgp on k_{off}**	**$TB_{PL}4$ Selected model**	**$TB_{PL}5$ slope = 0**
OFV	45677.7	45170.1	45166.6	45092.1	45536.9
AIC	45689.7	45184.1	45182.6	45108.1	45550.9
parameter	**Value (%CV)**	**Value (%CV)**	**Value (%CV)**	**Value (%CV)**	**Value (%CV)**
k_{off} (/min)	0.017 (8)	0.0103 (13)	0.0109 (17)	0.009 (26)	0.0149 (15)
k_{off} -Pgp (/min)	-	-	0.0087 (26)	-	-
K_D (nM)	1980 (37)	995 (36)	935 (37)	1570 (59)	3610
K_D -Pgp (nM)				381 (88)	715
E_0 (µV)	42.4 (4)	45.9 (4)	45.8 (4)	45.4 (4)	42.2
E_{max} (µV)	32.2 (14)	29.3 (13)	28.9 (13)	32.9 (20)	38.9
R_{tot} (nM)	1 FIX	1 FIX	1 FIX	1 FIX	1 FIX
slope (µV/min)	0 FIX	-0.0313 (13)	-0.0315 (12)	-0.0299 (12)	0 FIX
ω^2 E_0 (µV)	0.135 (18)	0.117 (20)	0.117 (20)	0.113 (19)	0.13 (17)
σ^2 proportional	0.0639 (6)	0.059 (6)	0.059 (6)	0.0584 (6)	0.0626 (6)

EC-TB_{PL} model fitting

The EC-TB_{PL} model structure that was tested to describe the EEG data is shown in Figure 3. The parameter values, OFVs and AICs are given in **Table 4**. Model EC-TB_{PL}1 was selected as best model on basis of the AIC, but this AIC is still 39 points higher than Model EC_{PL}1. The uncertainty in the parameter estimate of the K_D in the presence of the Pgp blocker (K_D –Pgp) is rather high with 93%, but this was allowed to test the conclusion that none of the binding models (TB_{PL}1 - TB_{PL}5 and EC-TB_{PL}1 - EC-TB_{PL}5) yielded lower AICs than the best effect compartment model (EC_{PL}1) in a conservative manner.

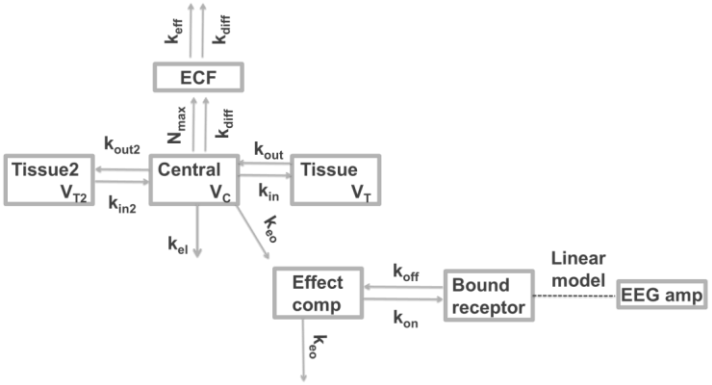

Figure 3. Schematic representation of the EC-TB_{PL} model structure that was used to describe the morphine EEG amplitudes over time. k_{on} is the second-order drug-target association rate constant. k_{off} is the first-order drug-target dissociation rate constant. k_{eo} is the first-order distribution rate constant into and out of the effect compartment. Target occupancy is linearly related to the EEG amplitude. The distribution from plasma to the tissue compartments and the brain ECF compartment is described in Supplement S 1. The arrows indicate morphine flows, the dotted line indicates a direct relationship.

Table 4. Parameter values and objective function values of the tested EC-TB_{PL} models describing the EEG data based on plasma concentrations. CV denotes the coefficient of variation as percentage. OFV denotes the Objective Function Value, AIC denotes the Akaike Information Criterion. ω^2 and σ^2 denote the variances of the exponential IIV distribution and the proportional error distribution, respectively.

	EC-TB_{PL}1 Selected model	EC-TB_{PL}2 no Pgp effect	EC-TB_{PL}3 Pgp on k_{eo}	EC-TB_{PL}4 k_{off} = 1	EC-TB_{PL}5 slope = 0
OFV	44790.9	44880.3	44873.8	45008.2	45235.3
AIC	44808.9	44896.3	44891.8	45024.2	45251.3
parameter	**Value (%CV)**	**Value (%CV)**	**Value (%CV)**	**Value (%CV)**	**Value (%CV)**
k_{off} (/min)	0.0275 (14)	0.0243 (14)	0.0247 (14)	1 FIX	0.0400 (9)
k_{eo} (/min)	0.0327 (17)	0.0365 (12)	0.0389 (14)	0.0162 (28)	0.036 (13)
k_{eo} -Pgp (/min)	-	-	0.0265 (31)	-	-
K_D (nM)	1520 (34)	1150 (30)	1110 (30)	2110 (50)	3150 (36)
K_D -Pgp (nM)	296 (93)	-	-	385 (78)	594 (47)
E_0 (µV)	45.0 (4)	45.7 (4)	45.6 (4)	45.2 (4)	41.9 (4)
E_{max} (µV)	31.8 (11)	30.7 (11)	30.5 (11)	34.4 (18)	37.3 (12)
R_{tot} (nM)	1 FIX	1 FIX	1 FIX	1 FIX	1 FIX
slope (µV/min)	-0.0276 (15)	-0.0296 (13)	-0.0296 (13)	-0.0273 (14)	0 FIX
ω^2 E_0 (µV)	0.111 (20)	0.116 (20)	0.116 (20)	0.111 (19)	0.129 (18)
σ^2 proportional	0.057 (7)	0.0565 (7)	0.0565 (7)	0.0576 (7)	0.0597 (7)

EC_{ECF}, TB_{ECF}, IE_{ECF} and DE_{ECF} model fitting

The last models that were fitted to the EEG data were based on the ECF concentrations instead of the plasma concentrations. Various model structures were tested, as shown in Figure 4. To compare the model fits based on ECF concentrations ($EC_{ECF}1$, $TB_{ECF}1$, $IE_{ECF}1$ and $DE_{ECF}1$) with the model fits that were based on plasma concentrations (EC_{PL}, TB_{PL} and EC-TB_{PL}), the best plasma model ($EC_{PL}1$) was fitted to the limited dataset that included only animals with ECF data. This model fit was compared to the ECF-based model fits on basis of their AICs, as shown in **Table 5**.

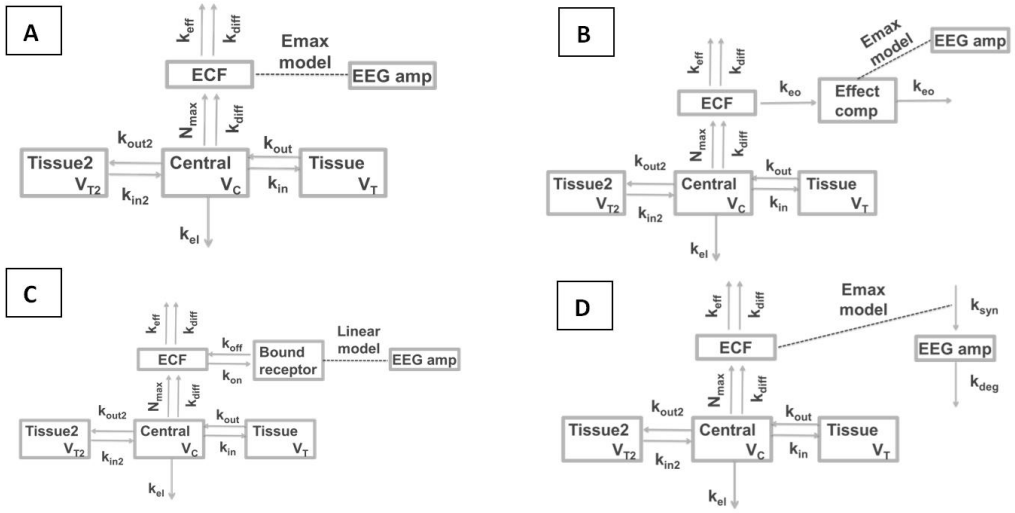

Figure 4. Schematic representation of the EC_{ECF}, TB_{ECF}, IE_{ECF} and DE_{ECF} model structures that were used to describe the EEG data based on brain ECF concentrations. The different structures represent A) the DE_{ECF} model, B) the EC_{ECF} model, C) the TB_{ECF} model and D) the IE_{ECF} model, with k_{syn} being the zero-order effect generation rate constant, and k_{deg} being the first-order effect degradation rate constant. The distribution from plasma to the tissue compartments and the brain ECF compartment is described in Supplement S 1. The arrows indicate morphine flows, the dotted line indicates a direct relationship.

Table 5. Parameter values and objective function values of the tested models describing the EEG data based on ECF concentrations. CV denotes the coefficient of variation as percentage. OFV denotes the Objective Function Value, AIC denotes the Akaike Information Criterion. ω^2 and σ^2 denote the variances of the exponential IIV distribution and the proportional error distribution, respectively.

[a] This value was estimated as the maximal k_{syn} minus baseline k_{syn} (calculated from E_0 and k_{deg}) and

	$EC_{PL}1$ ref. model	**$TB_{ECF}1$ binding model**	**$DE_{ECF}1$ direct effect**	**$EC_{ECF}1$ effect compartment**	**$IE_{ECF}1$ indirect effect**
OFV	25996.1	26284.1	26284.0	26255.1	26240.3
AIC	26118.1	26300.1	26300.0	26273.1	26258.3
parameter	**Value (%CV)**	**Value (%CV)**	**Value (%CV)**	**Value (%CV)**	**Value (%CV)**
k_{1e}(/min)	0.0457 (35)	-	-	-	-
k_{eo}(/min)	0.0377 (41)	-	-	0.161 (40)	-
k_{1e} -Pgp (/min)	0.0647 (36)	-	-	-	-
k_{eo} -Pgp (/min)	0.0155 (77)	-	-	-	-
E_0 (µV)	47.6 (6)	48.9 (6)	48.9 (6)	49.1 (6)	49.1 (6)
E_{max} (µV)	27.5 (20)	32.7 (17)	23.4 (18)	24.9 (19)	25.4[a] (36)
E_{max} –Pgp (µV)	-		41.6 (14)	43.2 (15)	43.3 (42)
EC_{50} (nM)	1100 (87)	-	173 (22)	182 (26)	182 (25)
N_H	2.05 (49)		2.3 (41)	2.02 (43)	2.07 (43)
slope (µV/min)	-0.0235 (34)	-0.0400 (17)	-0.0359 (17)	-0.0373 (19)	-0.0377 (19)
k_{off} (/min)	-	0.0932 (37)	-	-	-
K_D	-	283 (40)	-	-	-
K_D -Pgp	-	55.9 (15)	-	-	-
k_{deg} (/min)					0.124 (34)
ω^2 E_0 (µV)	0.0668	0.0668 (26)	0.072 (25)	0.0696 (26)	0.0961 (26)
σ^2 proportional	0.0550 (10)	0.0598 (10)	0.0598 (10)	0.0593 (10)	0.059 (10)

calculated by dividing the estimated value by the k_{deg}.

Of all the models that are described above, model $EC_{PL}1$ has the lowest AIC. To evaluate its performance in more detail, the most relevant diagnostic plots are given in Figure S 6 to Figure S 10. These diagnostic plots indicate that the main trend of the data is captured, although the obtained fit is not optimal (which is especially clear from Figure S 10). The small difference in AIC between the best combined EC-TB model ($EC\text{-}TB_{PL}1$) and the best EC model ($EC_{PL}1$) is also reflected by very similar VPC results, as shown in Figure S 11. Moreover, the best model with only binding from plasma($TB_{PL}4$) also provided a similar VPC result (see Figure S 12).

Dose-dependency of $Tmax_{TO}$ in a TB_{PL} model

Our simulations of drug-target binding in a TB_{PL} model for the range of the most relevant binding kinetics demonstrated that the observable influence of dose on $Tmax_{TO}$, which discriminates the TB model from the EC model, is limited to a confined range of k_{on} and k_{off} combinations. As visualized in Figure 5, if the k_{off} has a value around the elimination rate constant of 0.03/hr $\Delta Tmax_{TO}$ is maximal. Also, the initial drug concentration C0 should not be above a specific threshold value which is approximately equal to the target concentration. The absolute $\Delta Tmax_{TO}$ for different doses (as shown in Figure 5) will be most relevant for the identification of the dose-dependent $\Delta Tmax_{TO}$ in a PKPD modelling study. However, for the understanding of the underlying determinants of this shift in $\Delta Tmax_{TO}$, the ratio of the $\Delta Tmax_{TO}$ values belonging to the 2 doses should also be considered, as shown in Figure 6. For example, if the two different $Tmax_{TO}$ values obtained from the two doses are 1 and 3 minutes, their ratio is 3, but the absolute difference is 2 minutes. If the two $Tmax_{TO}$ values are 1 and 3 hours, their ratio is still 3, but the difference is now 2 hours. In this latter case, the influence of the dose on the $Tmax_{TO}$ will be more easily identified. Representative example simulations that can help to understand the characteristics of Figure 5 are provided in Supplement S 2.

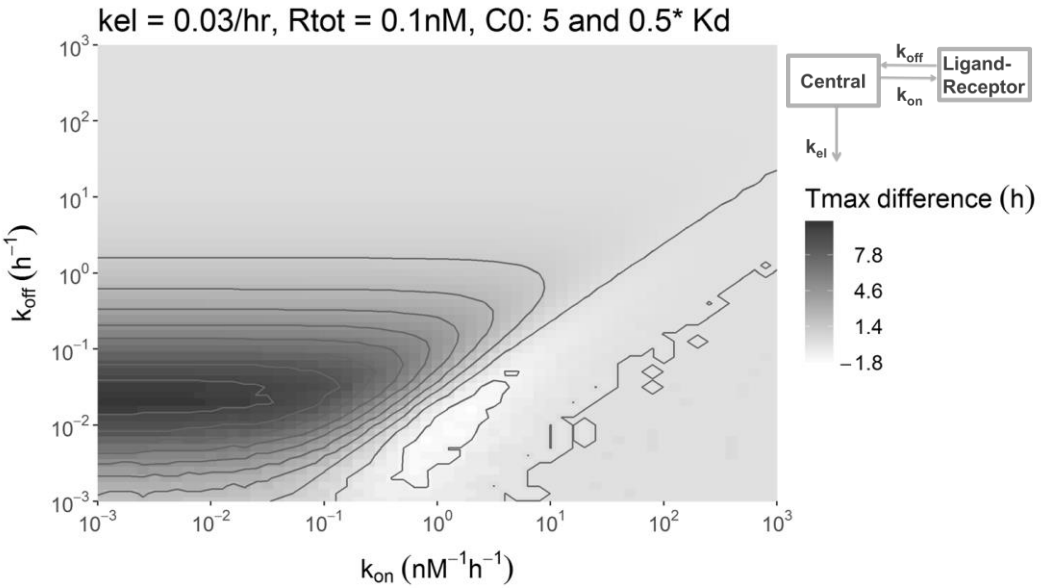

Figure 5. Overview of the shift in $Tmax_{TO}$ that was observed in the simulations with the TB_{PL} model (see upper-right corner) as a result of the change in the affinity-normalized dose (leading to an initial concentration of 5 and 0.5 times the K_D). The elimination rate constant k_{el} was 0.03/hr and the target concentration was 0.1 nM for all simulations in this figure.

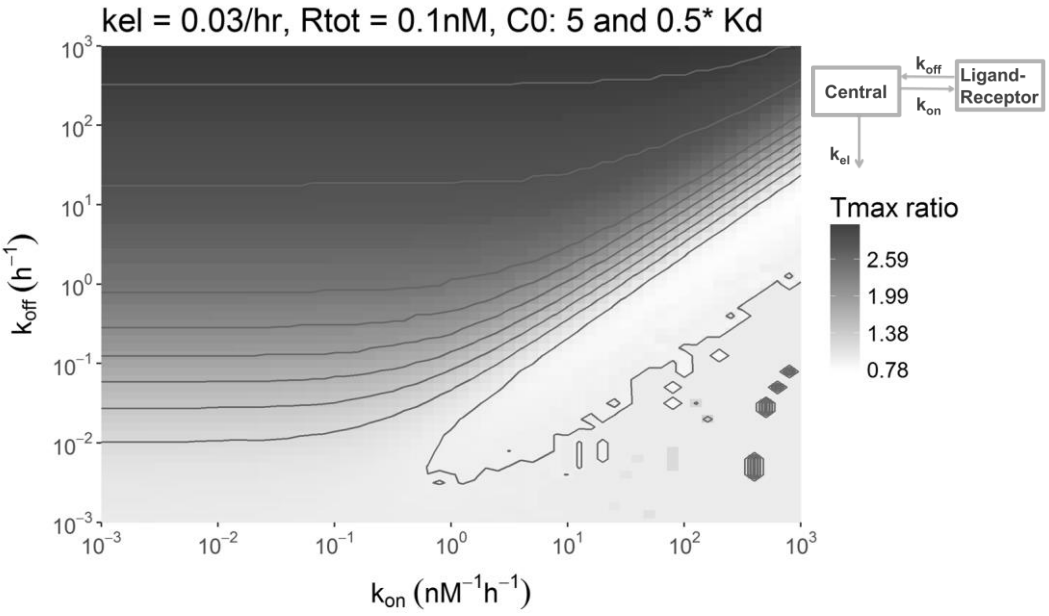

Figure 6. Overview of the ratio of $Tmax_{TO}$ values that was observed in the simulations with the TB_{PL} model (see inset) as a result of the change in the affinity-normalized dose (leading to an initial concentration of 5 and 0.5 times the K_D). The elimination rate constant k_{el} was 0.03/hr and the target concentration was 0.1 nM for all simulations in this figure.

Interestingly, the relationship between the $\Delta Tmax_{TO}$, the elimination rate constant, the target concentration and the dose could be approximated mathematically for the upper region, the lower-left region and the lower-right region of Figure 5 as presented in Supplement S 3. From this analysis, it follows that for the upper half of Figure 5, where the k_{off} is much larger than the k_{el}, $Tmax_{TO}$ is always small, and a significant $\Delta Tmax_{TO}$ will thus not be observed. For the lower and the lower-right part of Figure 5, where the k_{off} is much smaller than the k_{el}, it is found that $Tmax_{TO}$ does not depend on the dose. More specifically, when the initial drug concentration is much lower than the target concentration (and k_{off} is smaller than k_{el}), the $Tmax_{TO}$ is merely determined by the k_{el}. On the other hand, when the initial drug concentration is much larger than the target concentration (and k_{off} is smaller than k_{el}), the $Tmax_{TO}$ is given by a relation between k_{off} and k_{el}. This relationship between the $\Delta Tmax_{TO}$, the elimination rate constant, the target concentration and the dose is illustrated in Figure 7.

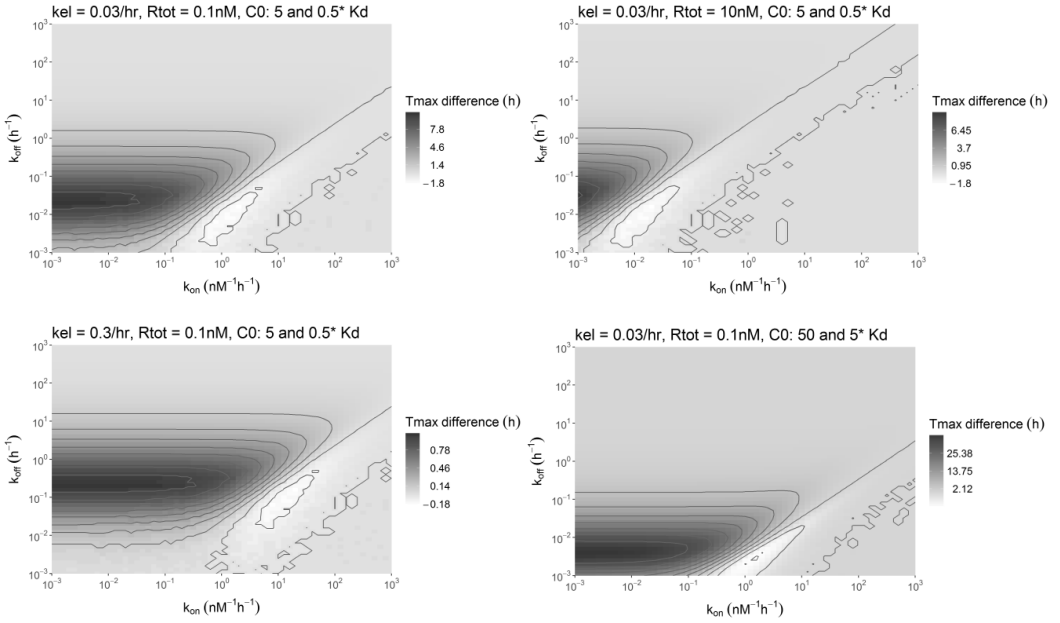

Figure 7. Overview of the $\Delta Tmax_{TO}$ that was observed in the simulations as a result of the change in the affinity-normalized dose for different combinations of parameter values as indicated above the panels. All panels vary only one parameter compared to the upper left panel.

Discussion

In this study, we compared TB and EC models to describe the delay between morphine plasma concentrations and EEG effects for 3 different dose levels. We found that model discrimination was difficult to obtain and that selection of the best model (the EC_{PL} model in this study) was only possible on basis of the objective function value differences. Moreover, our simulation study with the TB_{PL} model showed that a shift in $Tmax_{TO}$ with increasing doses, the distinctive future of the TB model compared to the EC model, only occurs for a limited range in parameter values. Both a k_{off} value much smaller and much larger than the k_{el} value and a target concentration larger than the initial drug concentration decrease this shift in $Tmax_{TO}$ towards zero.

Since our model simulations show that the $Tmax_{TO}$ does not depend on the dose for k_{off} values much lower than the k_{el} and target concentrations much higher than the initial drug concentration, this means that the TB_{PL} model for these parameter values behaves like an EC_{PL} model, with a first order increase and decrease in the concentration that is linked to the effect. Together with the small differences in EC and TB model fits

to the morphine EEG data, this shows that for many parameter combinations, a TB model gives rise to similar drug effect profiles as an EC model. This means that neither a successful fit of a TB or EC model necessarily supports the relevance of target binding or target site distribution, respectively, while a single successful fit is often presented as such support[11,23,39]. To obtain support for one of the two mechanisms, both models should be fitted to the data and compared on basis of objective metrics such as the AIC. This approach demonstrated the added value of the combined EC-TB_{PL} model compared to the EC_{PL} and the TB_{PL} model for buprenorphine and AR-HO47108.[13,29] However, this method also demonstrated that the TB_{PL} model performed similarly as the EC_{PL} model for eight calcium antagonists[14] and that the EC model performed similarly as the EC-TB_{PL} model for fentanyl [13]. This demonstrates that even if objective metrics are used, discrimination between two models is not always possible. Moreover, obtained model discrimination strictly informs on the data fit of each model, not directly on the plausibility of the represented mechanism. The TB model should be considered and tested more often as alternative to the EC model, as its parameters can be measured *in vitro*/*ex vivo*, which enables a better *in vitro-in vivo* extrapolation (IVIVE).

In this study, we also found that the models based on brain ECF concentrations did not perform better than the models based on plasma concentrations. One would expect that the brain ECF concentrations would reflect the target site concentration better than the plasma concentrations, especially if brain distribution is relatively slow and nonlinear, as it was in this study. The inferior performance of the brain ECF-based models might be explained by the extremely high variability in the brain ECF data of the 4 mg/kg dose group, as shown in Figure S 5. However, a direct effect model ($DE_{ECF}1$) could be identified from the brain ECF concentrations and showed an only 39 points higher AIC than the best model $IE_{ECF}1$, while such a model fit could not be obtained from the plasma concentrations, indicating that the ECF concentrations reflect the target site concentration more closely compared to the plasma concentrations. This is in line with the relevance of drug concentrations in the brain for CNS effects that has been demonstrated by several other studies[40–43] and the difference between plasma and brain concentrations that has been identified for several compounds[44]. In all our target binding models, a linear target occupancy-effect relationship had to be assumed to keep the model parameters identifiable. Such a linear relationship has been observed and can be expected unless for full agonists in tissues with relatively high target concentrations compared to the concentration of signal transduction molecules (i.e. for a high receptor reserve).[24]

Only a one compartment pharmacokinetic model was used in this study in combination with the simplest TB_{PL} model to investigate the $\Delta Tmax_{TO}$. We expect that the same principles apply if the TB_{PL} model has a two-compartment or three compartment pharmacokinetic models or with target turnover or signal transduction models, but the parameter range for which $Tmax_{TO}$ shifts with a change in dose might be different compared to the model used in our simulations. In analogy to Figure 7, for the combined EC-TB model one would expect that to obtain a significant $\Delta Tmax_{TO}$ and to identify the TB model in addition to the EC model, the k_{e0} should be in the same order of magnitude as the k_{off} if the maximal drug concentration is around or below the K_D. This is indeed the case for the two successful examples of a EC-TB_{PL} fit: for buprenorphine, the k_{e0} was 0.0242 min^{-1} and the k_{off} was 0.0731 min^{-1}[13] and for AR-HO47108, the k_{e0} was 0.0351 for the drug and 0.00749 for its metabolite and the k_{off} was 0.00303 min^{-1} and 0.00827 min^{-1}, respectively[29]. On the other hand, the combined EC-TB model EC-$TB_{PL}1$ that was identified in this study for morphine also showed a similar value for k_{e0} and k_{off} (0.0327 and 0.275, respectively), but this model was not better than the EC model $EC_{PL}1$. In comparison with our one compartment PK model with intravenous dosing, especially the absorption or the distribution phase into the target site could pose additional limiting factors that prevent a shift in $Tmax_{TO}$ with increasing doses.

One of the most important advantages of the EC model is that it only requires one parameter, k_{e0}. However, the EC model most often needs to be combined with an Emax model, which also requires two or three parameters, Emax, EC_{50} and possibly the hill factor. The binding model has 3 parameters, k_{on}, k_{off} and R_{tot}, and needs at least 1 additional parameter, Emax, to convert occupancy predictions to effect predictions. One or two additional parameters might be required to describe a nonlinear target occupancy-effect relationship, which is required in case of a high efficacy and receptor reserve[24]. The discrimination between the two nonlinearities in such cases might be hard or impossible to obtain. However, k_{on} and k_{off}

can be obtained from in vitro experiments and R_{tot} from *ex vivo* experiments. Especially the identification of R_{tot} from *ex vivo* data can help to reduce the difficulties with parameter identifiability as often associated with the TB model [45].

In summary, the limited difference between TB and EC models should be taken into account in the evaluation of historical and the design of new modelling studies. By informing the TB models with *in vitro* data, TB models can help to translate between *in vitro* and *in vivo* studies. The combination of parameter values for which the $Tmax_{TO}$ in the target binding model is dependent on the dose is limited to k_{off} values around the elimination rate constant and to target concentrations lower than the initial drug concentration. Although the combination of multi-compartment PK models, TB models and target turnover models might affect the parameter range were the $Tmax_{TO}$ is dependent on the dose, our study is a first indication that such limitations should be taken into account for understanding TB models.

Conclusion

In this study, we have shown that successful fitting of a TB or EC model is not enough support to assume the relevance of target binding or target site distribution. Moreover, we have shown for a one-compartment pharmacokinetic model with target binding that the $\Delta Tmax_{TO}$ for changing doses can only be identified if the k_{off} has a value around the pharmacokinetic elimination rate constant and the target concentration is lower than the initial drug concentration. We have thus identified that the $Tmax_{TO}$ is determined by the rate of target binding relative to the decline rate of unbound drug and unbound target concentrations. Our findings indicate that the relatively sparse occurrence of target binding models in literature does not discredit the relevance of target binding kinetics. Our study also shows that a TB and EC model might be similar for the tested dose range and pharmacokinetic conditions, while extrapolation to different conditions might result in different effect *versus* time profiles for the TB and EC model. We conclude that identification of the appropriate model is important and that target binding models should be tested more often to increase the translation between *in vitro* and *in vivo* studies and to increase the predictive power of developed PKPD models.

References

1. Copeland RA, Pompliano DL, Meek TD. Drug-target residence time and its implications for lead optimization. Nat Rev Drug Discov 2006;5(9):730–9
2. Lu H, Tonge PJ. Drug-Target Residence Time: Critical Information for Lead Optimization. Curr Opin Chem Biol 2011;14(4):467–74
3. Dahl G, Akerud T. Pharmacokinetics and the drug-target residence time concept. Drug Discov Today 2013;18(15–16):697–707
4. Schuetz DA, de Witte WEA, Wong YC, et al. Kinetics for Drug Discovery: an industry-driven effort to target drug residence time. Drug Discov Today 2017;22(6):896–911
5. de Witte WEA, Wong YC, Nederpelt I, et al. Mechanistic models enable the rational use of in vitro drug-target binding kinetics for better drug effects in patients. Expert Opin Drug Discov 2016;11(1):45–63
6. de Witte WEA, Danhof M, van der Graaf PH, et al. In vivo Target Residence Time and Kinetic Selectivity: The Association Rate Constant as Determinant. Trends Pharmacol Sci 2016;37(10):831–42
7. Vauquelin G, Bostoen S, Vanderheyden P, et al. Clozapine, atypical antipsychotics, and the benefits of fast-off D2 dopamine receptor antagonism. Naunyn Schmiedebergs Arch Pharmacol 2012;385(4):337–72
8. Sahlholm K, Zeberg H, Nilsson J, et al. The fast-off hypothesis revisited: A functional kinetic study of antipsychotic antagonism of the dopamine D2 receptor. Eur Neuropsychopharmacol 2016;26(3):467–76
9. Ramsey SJ, Attkins NJ, Fish R, et al. Quantitative pharmacological analysis of antagonist binding kinetics at CRF1 receptors in vitro and in vivo. Br J Pharmacol 2011;164(3):992–1007
10. Jiang XL, Samant S, Lewis JP, et al. Development of a physiology-directed population pharmacokinetic and pharmacodynamic model for characterizing the impact of genetic and demographic factors on clopidogrel response in healthy adults. Eur J Pharm Sci 2016;82:64–78
11. Hong Y, Gengo FM, Rainka MM, et al. Population pharmacodynamic modelling of aspirin- and ibuprofen-induced inhibition of platelet aggregation in healthy subjects. Clin Pharmacokinet 2008;47(2):129–37
12. Äbelö A, Holstein B, Eriksson UG, et al. Gastric acid secretion in the dog: A mechanism-based pharmacodynamic model for histamine stimulation and irreversible inhibition by omeprazole. J Pharmacokinet Pharmacodyn 2002;29(4):365–82
13. Yassen A, Olofsen E, Dahan A, et al. Pharmacokinetic-Pharmacodynamic Modeling of the Antinociceptive Effect of Buprenorphine and Fentanyl in Rats : Role of Receptor Equilibration Kinetics. J Pharmacol Exp Ther 2005;313(3):1136–49
14. Shimada S, Nakajima Y, Yamamoto K, et al. Comparative Pharmacodynamics of Eight Calcium Channel Blocking Agents in Japanese Essential Hypertensive Patients. Biol Pharm Bull 1996;19(3):430–7
15. Dua P, Hawkins E, van der Graaf P. A Tutorial on Target-Mediated Drug Disposition (TMDD) Models. CPT Pharmacometrics Syst Pharmacol 2015;4(6):324–37
16. Lammertsma AA, Hume SP. Simplified reference tissue model for PET receptor studies. Neuroimage 1996;4:153–8
17. Liefaard LC, Ploeger BA, Molthoff CFM, et al. Population pharmacokinetic analysis for simultaneous determination of Bmax and KD in vivo by positron emission tomography. Mol imaging Biol 2005;7(6):411–21
18. Louizos C, Yáñez JA, Forrest ML, et al. Understanding the hysteresis loop conundrum in pharmacokinetic / pharmacodynamic relationships. J Pharm Pharm Sci 2014;17(1):34–91
19. Upton R, Mould D. Basic Concepts in Population Modeling, Simulation, and Model-Based Drug Development: Part 3—Introduction to Pharmacodynamic Modeling Methods. CPT Pharmacometrics Syst Pharmacol 2014;3(1)
20. Holford NHG, Sheiner LB. Understanding the Dose-Effect Relationship: Clinical Application of Pharmacokinetic-Pharmacodynamic Models. Clin Pharmacokinet 1981;6:429–53
21. Jusko WJ, Ko HC. Physiologic indirect response models characterize diverse types of pharmacodynamic effects. Clin Pharmacol Ther 1994;56(4):406–19
22. Paton WDM. A theory of drug action based on the rate of drug-receptor combination. Proc R Soc London Ser B Biol Sci 1961;154(954):21–69
23. Perry DC, Mullis KB, Oie S, et al. Opiate antagonist receptor binding in vivo: evidence for a new receptor binding model. Brain Res 1980;199(1):49–61
24. Ruffolo RR. Important Concepts of Receptor Theory. J Auton Pharmacol 1982;2(4):277–95
25. Wakelkamp M, Alvá N G, Paintaud G. The time of maximum effect for model selection in pharmacokinetic–pharmacodynamic analysis applied to frusemide. Br J Clin Pharmacol 1998;45:63–70
26. Ploeger BA, Van Der Graaf PH, Danhof M. Incorporating Receptor Theory in Mechanism-Based Pharmacokinetic-Pharmacodynamic (PK-PD) Modeling. Drug Metab Pharmacokinet 2009;24(1):3–15
27. N.L.Dayneka, Garg V, W.J.Jusko. Comparison of four basic models of indirect pharmacodynamic responses. J Pharmacokinet Biopharm 1993;21(4):457–77
28. Peletier LA, Gabrielsson J, Haag J Den. A dynamical systems analysis of the indirect response model with special emphasis on time to peak response. J Pharmacokinet Pharmacodyn 2005;32(3–4):607–54

29. Äbelö A, Andersson M, Holmberg AA, et al. Application of a combined effect compartment and binding model for gastric acid inhibition of AR-HO47108: A potassium competitive acid blocker, and its active metabolite AR-HO47116 in the dog. Eur J Pharm Sci 2006;29(2):91–101
30. Yassen A, Olofsen E, Kan J, et al. Animal-to-human extrapolation of the pharmacokinetic and pharmacodynamic properties of buprenorphine. Clin Pharmacokinet 2007;46(5):433–47
31. Cleton A, de Greef HJ, Edelbroek PM, et al. Application of a combined "effect compartment/indirect response model" to the central nervous system effects of tiagabine in the rat. J Pharmacokinet Biopharm 1999;27(3):301–23
32. Jusko WJ, Ko HC, Ebling WF. Convergence of direct and indirect pharmacodynamic response models. J Pharmacokinet Biopharm 1995;23(1):5–8
33. Hutmacher MM, Mukherjee D, Kowalski KG, et al. Collapsing mechanistic models: An application to dose selection for proof of concept of a selective irreversible antagonist. J Pharmacokinet Pharmacodyn 2005;32(3–4):501–20
34. Groenendaal D, Freijer J, de Mik D, et al. Influence of biophase distribution and P-glycoprotein interaction on pharmacokinetic-pharmacodynamic modelling of the effects of morphine on the EEG. Br J Pharmacol 2007;151(5):713–20
35. Groenendaal D, Freijer J, de Mik D, et al. Population pharmacokinetic modelling of non-linear brain distribution of morphine: influence of active saturable influx and P-glycoprotein mediated efflux. Br J Pharmacol 2007;151:701–12
36. Beal S, Sheiner LB, Boeckmann A, et al. NONMEM 7.3.0 Users Guides. (1989-2013). Icon Development Solutions,;
37. Akaike H. Information Theory and an Extension of the Maximum Likelihood Principle. In: Kotz S, Johnson NL, editors. Breaktroughs in Statistics, Vol I, Foundations and Basic Theory New York; 1992. p. 610–24
38. Zhang L, Beal SL, Sheiner LB. Simultaneous vs . Sequential Analysis for Population PK / PD Data I: Best-case Performance. J Pharmacokinet Pharmacodyn 2003;30(6):387–404
39. Walkup GK, You Z, Ross PL, et al. Translating slow-binding inhibition kinetics into cellular and in vivo effects. Nat Chem Biol 2015;11(6):416–23
40. Stevens J, Ploeger BA, Hammarlund-Udenaes M, et al. Mechanism-based PK-PD model for the prolactin biological system response following an acute dopamine inhibition challenge: quantitative extrapolation to humans. J Pharmacokinet Pharmacodyn 2012;39(5):463–77
41. Larsen MS, Keizer R, Munro G, et al. Pharmacokinetic/Pharmacodynamic Relationship of Gabapentin in a CFA-induced Inflammatory Hyperalgesia Rat Model. Pharm Res 2016;33(5):1133–43
42. Danhof M, Levy G. Kinetics of Drug Action in Disease States. I. Effect of Infusion Rate on Phenobarbital Concentrations in Serum, Brain and Cerebrospinal Fluid of Normal Rats at Onset of Loss of Righting Reflex1. J Pharmacol Exp Ther 1984;229(1):44–50
43. Balerio GN, Rubio MC. Pharmacokinetic-Pharmacodynamic Modeling of the antinociceptive effect of baclofen in mice. Eur J Drug Metab Pharmacokinet 2002;27(3):163–9
44. Yamamoto Y, Välitalo PA, van den Berg D-J, et al. A Generic Multi-Compartmental CNS Distribution Model Structure for 9 Drugs Allows Prediction of Human Brain Target Site Concentrations. Pharm Res 2017;34(2):333–51
45. Janzén DLI, Bergenholm L, Jirstrand M, et al. Parameter identifiability of fundamental pharmacodynamic models. Front Physiol 2016;7(DEC):1–12
46. Tummino PJ, Copeland RA. Residence Time of Receptor-Ligand Complexes and Its Effect on Biological Function. Biochemistry 2008;47(20):5481–92

Supplement S 1. Morphine PK and PD model fits, GOF plots and VPCs

Plasma concentration modelling

A three-compartment model (Figure S 1) was identified as the best model with respect to the AIC and the individual fits. The goodness of fit of this model is illustrated in Figure S 2 and Figure S 3.

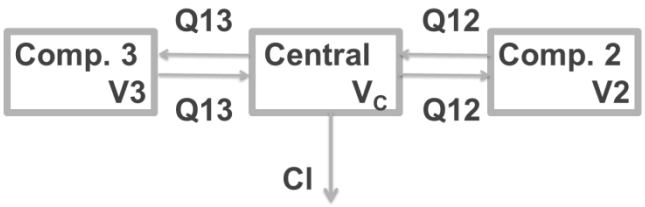

Figure S 1. Schematic representation of the three-compartment model structure that was used to describe the morphine plasma concentrations over time.

The differential equations of the model in Figure S 1 are given in equations 1-3. In these equations, A_c, A_2 and A_3 represent the amount of drug in the central, second and third compartment, respectively. k_{el} k_{12}, k_{21} k_{13} and k_{31} represent the first order rate constants of elimination and distribution between the compartments. The relation between the parameters in equations 1-3 and the estimated parameters as given in Table S 1 is shown in equation 4-8. V_c, V_2 and V_3 represent the volumes of the respective compartments and CL, Q12 and Q13 represent the clearances of elimination and distribution between compartments.

1. $\frac{dA_c}{dt} = -k_{el} \cdot A_c - k_{12} \cdot A_c - k_{13} \cdot A_c + k_{21} \cdot A_2 + k_{31} \cdot A_3$
2. $\frac{dA_2}{dt} = k_{12} \cdot A_c - k_{21} \cdot A_2$
3. $\frac{dA_3}{dt} = k_{13} \cdot A_c - k_{31} \cdot A_3$
4. $k_{el} = \frac{CL}{V_c}$
5. $k_{12} = \frac{Q12}{V_c}$
6. $k_{13} = \frac{Q13}{V_c}$
7. $k_{21} = \frac{Q12}{V_2}$
8. $k_{31} = \frac{Q13}{V_3}$

The goodness of fit of this model is illustrated in Figure S 2 and Figure S 3. Inter individual variability (IIV) was estimated for 4 of the estimated model parameters. Attempts to add IIV on more parameters resulted in a failing covariance step while the drop in OFV was limited (9 points). Comparison to the 2-compartment model with the lowest OFV value that was tested demonstrated better individual fits and a 109-points lower OFV for the 3-compartment model.

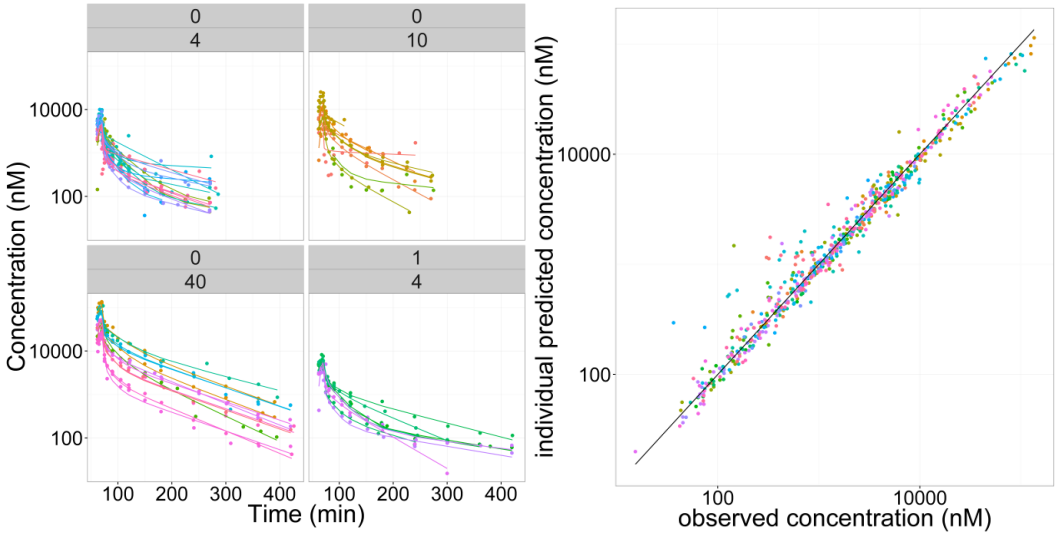

Figure S 2. Diagnostic plots of the plasma concentration fits. Left panel: Overview of observed (dots) and predicted (lines) concentrations. Upper panel labels indicate the dose in mg/kg and lower panel labels the presence (1) or absence (0) of Pgp inhibitor GF120918. Right panel: relation between observed and individual predicted plasma concentrations on a double logarithmic scale.

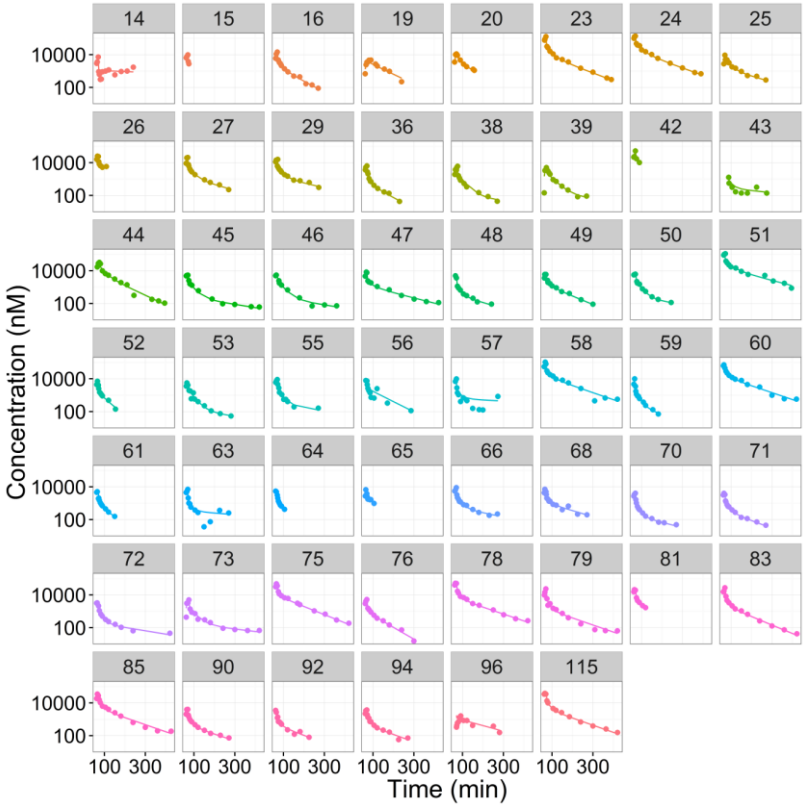

Figure S 3. Individual profiles of observed (dots) and predicted (lines) concentrations on a semi-logarithmic scale. Panel labels indicate the animal ID number.

Table S 1. Parameter values and objective function values of the tested models for the plasma concentrations. CV denotes the coefficient of variation as percentage. OFV denotes the Objective Function Value. ω^2 and σ^2 denote the variances of the exponential IIV distribution and the error distribution, respectively.

	2-cmp model	**3-cmp model 4 IIV parameters**	**3-cmp model 5 IIV parameters**
OFV	9314	9205	9194
parameter	**Value (CV)**	**Value (CV)**	**Value (CV)**
CL (L/min)	0.0300 (8)	0.028 (22)	0.028
V1 (L)	0.200 (11)	0.17 (49)	0.12
Q12 (L/min)	0.0432 (10)	0.019 (66)	0.056
V2 (L)	1.15 (10)	1.3 (48)	0.51*
Q13 (L/min)	-	0.031 (30)	0.020
V3 (L)	-	0.36 (32)	1.4*
ω^2 CL	0.34 (23)	0.33 (25)	0.35
ω^2 V1	0.55 (27)	0.63 (35)	0.15
ω^2 Q12	0.28 (39)	0.62 (33)	0.72
ω^2 V2	0.32 (31)	0.66 (28)	0 FIX
ω^2 Q13			0.79
ω^2 V3			0.57
σ^2 proportional	0.0766 (15)	0.79 (14)	0.071
σ^2 additive	1710 (28)	0 FIX	7.2

* To get the best model fit, V2 and V3 were estimated here as the ratio of V2 and V1 and the ratio of V3 and V2, respectively. The displayed values in this table are derived from the estimated ratios. CV = coefficient of variation as percentage.

ECF concentration modelling

Various structural models were tested for the description of the ECF concentrations, including a two-compartent model (ECF and "deep brain") and a target binding model (ECF-unbound and ECF bound). The best combination of OFV, parameter estimate uncertainty and diagnostic plots was obtained with the original one compartment ECF model, with passive first-order in- and outward distribution, saturable influx and first-order efflux (Figure S 4). As the parameters for the plasma concentrations were fixed, the only additional equation is given in equation 9, in which A_{ECF} and V_{ECF} refer to the amount and volume of the ECF compartment, respectively, k_{diff} and k_{eff} represent first order influx and efflux rate constants, Nmax represents the maximal saturable influx rate and C_{50} is the plasma concentration at which the saturable influx is half-maximal.

$$9. \quad \frac{d\frac{A_{ECF}}{V_{ECF}}}{dt} = k_{diff} \cdot \left(\frac{A_1}{V_1} - \frac{A_{ECF}}{V_{ECF}}\right) + \frac{N_{max} \cdot \frac{A_1}{V_1}}{C_{50} + \frac{A_1}{V_1}} - k_{eff} \cdot \frac{A_{ECF}}{V_{ECF}}$$

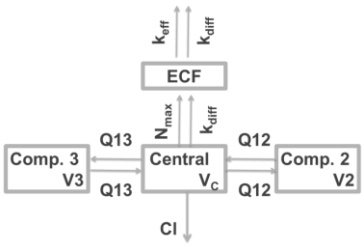

Figure S 4. Schematic representation of the model structure that was used to describe the morphine ECF concentrations over time. k_{diff} = first-order in- and outward distribution rate constant. k_{eff} first-order efflux rate constant. Nmax = zero-order maximal saturable influx rate constant.

Different versions of this model were tested in which the inter-individual variability was tested on different parameters and the influence of Pgp was estimated. Estimating the influence of Pgp did not reduce the OFV enough, so the final model did not include the influence of Pgp and had IIV estimated for k_{diff} and N_{max}. The diagnostic plots for the evaluation of the fit of this model is given in Figure S 5.

Table S 2. Parameter values and objective function values of the tested models for the ECF concentrations. CV denotes the coefficient of variation as percentage. OFV denotes the Objective Function Value. ω^2 and σ^2 denote the variances of the exponential IIV distribution and the error distribution, respectively.

	IIV on k_{diff}, N_{max}	**IIV on k_{diff}, k_{eff}**	**IIV on k_{diff}, k_{eff} Pgp on N_{max}**	**IIV on k_{diff}, N_{max} Pgp on N_{max}**
OFV	-1126	-1096	-1104	-1128
parameter	**Value (CV)**	**Value (CV)**	**Value (CV)**	**Value (CV)**
k_{diff}(/min)	0.0025 (17)	0.0027 (19)	0.0027 (17)	0.0025 (16)
k_{eff}(/min)	0.020 (11)	0.021 (20)	0.0213 (24)	0.019 (12)
N_{max} (nM/min)	2.6 (21)	3.0 (38)	2.2 (34)	2.2 (29)
N_{maxPgp} (nM/min)	-	-	4.45 (52)	3.15 (28)
ω^2 k_{diff}	0.36 (39)	0.44 (47)	0.44 (45)	0.35 (39)
ω^2 k_{eff}	0 FIX	0.35 (108)	0.31 (71)	0 FIX
ω^2 N_{max}	0.42 (55)	0 FIX	0 FIX	0.39 (52)
σ^2 proportional	0.11 (18)	0.11 (22)	0.11 (22)	0.11 (20)

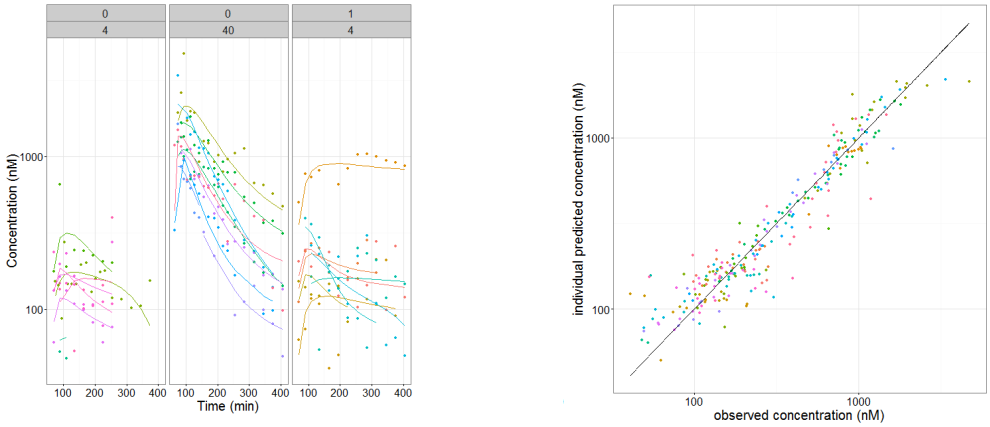

Figure S 5. Diagnostic plots of the ECF concentration fits. Left panel: Overview of observed (dots) and predicted (lines) concentrations. lower panel labels indicate the dose in mg/kg and upper panel labels the presence (1) or absence (0) of Pgp inhibitor GF120918. Right panel: relation between observed and individual predicted plasma concentrations on a double logarithmic scale.

EEG effect modelling

Model equations, Goodness of fit and VPC for model $EC_{PL}1$

The model equations for the connection between plasma concentrations and EEG effect are given in equations 10-12, where A_{TRANS} and V_{TRANS} refer to the amount of drug and the volume of the transit compartment, A_{EFF} and V_{EFF} refer to the amount of drug and the volume of the effect compartment k_{1e} and k_{e0} refer to the first order distribution rate constants into and out of the transit and effect compartment, E0 is the baseline EEG amplitude, slope is the linear change of the EEG amplitude during the experiment without morphine treatment, Emax is the maximal increase in EEG amplitude due to morphine, N_H is the hill coefficient and EC_{50} is the morphine plasma concentration that leads to the half-maximal increase in EEG amplitude.

10. $$\frac{d\frac{A_{TRANS}}{V_{TRANS}}}{dt} = k_{1e} \cdot \left(\frac{A_1}{V_1} - \frac{A_{TRANS}}{V_{TRANS}}\right)$$

11. $$\frac{d\frac{A_{EFF}}{V_{EFF}}}{dt} = k_{1e} \cdot \left(\frac{A_{TRANS}}{V_{TRANS}}\right) - k_{e0} \cdot \frac{A_{EFF}}{V_{EFF}}$$

12. $$Effect\ (EEG\ amplitude) = E_0 + slope * t + \frac{E_{max} \cdot \left(\frac{A_{EFF}}{V_{EFF}}\right)^{N_H}}{EC_{50}{}^{N_H} + \left(\frac{A_{EFF}}{V_{EFF}}\right)^{N_H}}$$

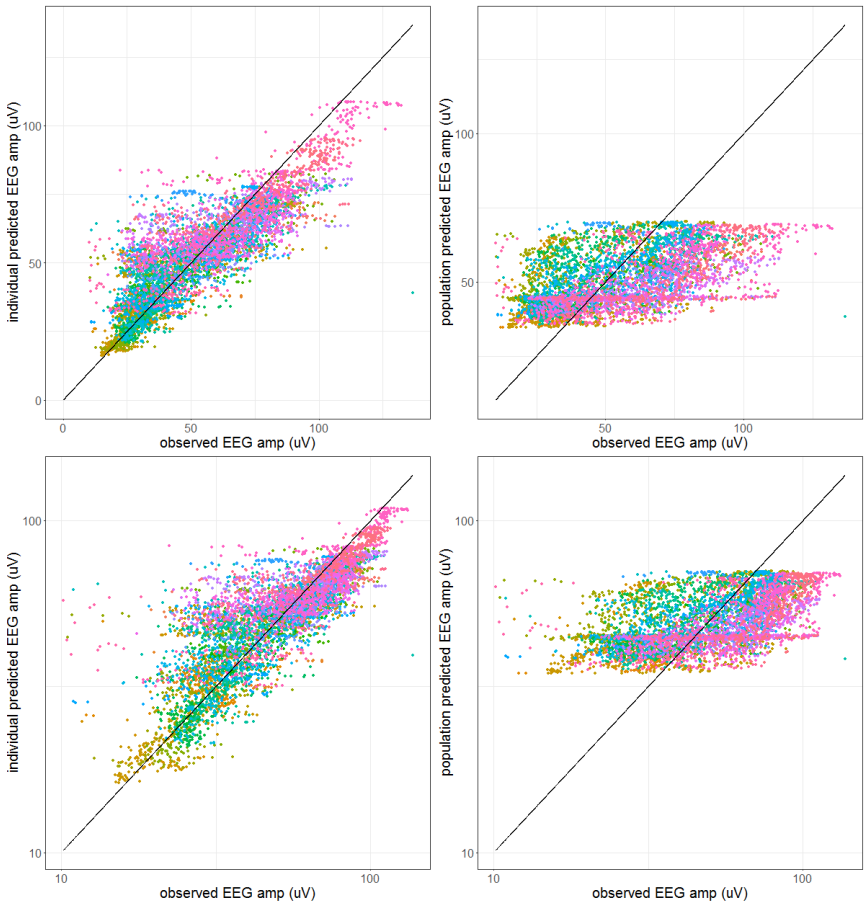

Figure S 6. Population (right panels) and individual (left panels) observed versus predicted EEG data as obtained from the model fit of model $EC_{PL}1$. The upper panels have a linear scale and the lower panels have a logarithmic scale.

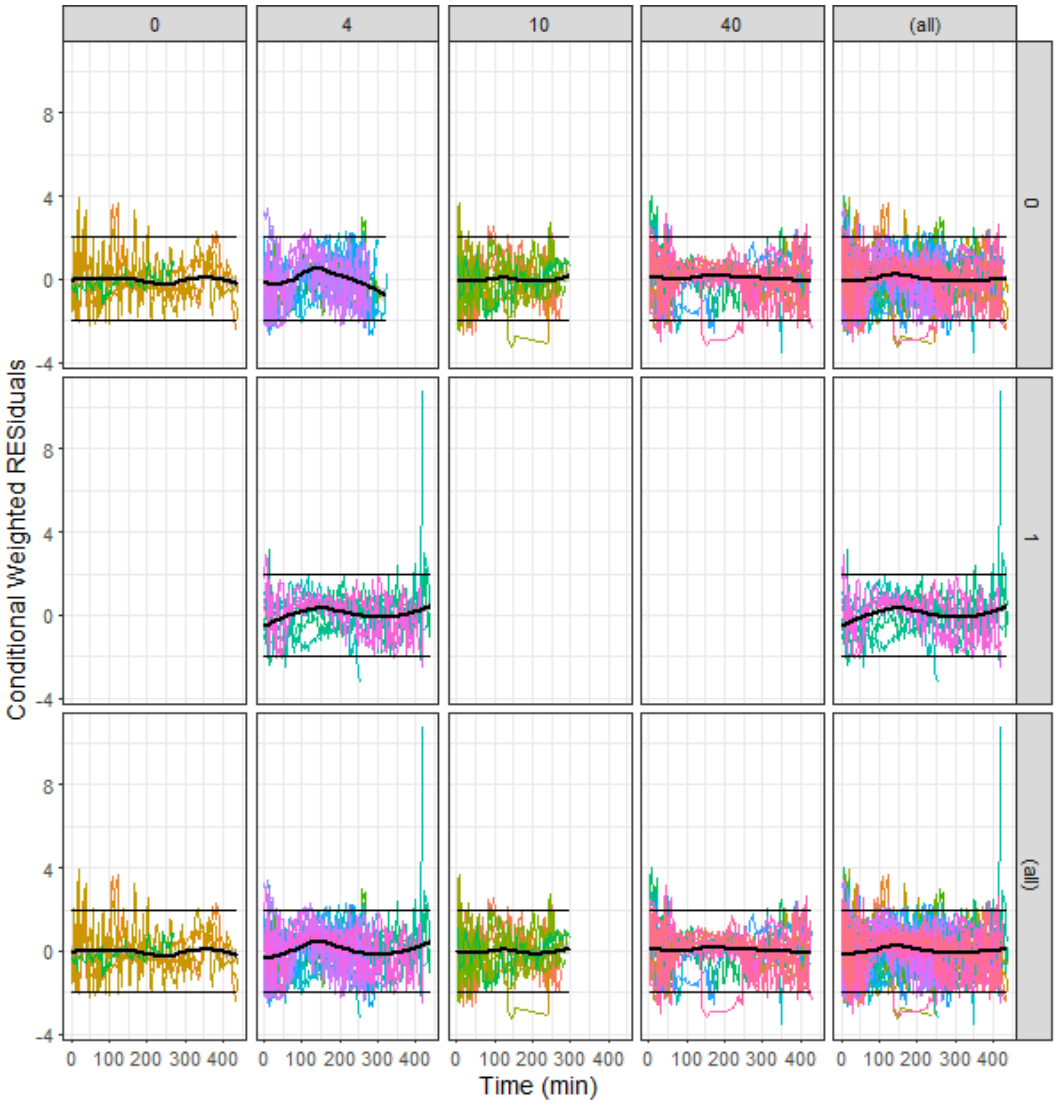

Figure S 7. Conditional weighted residuals versus time for the different dose groups and dose group combinations in the model fit of $EC_{PL}1$. The top labels indicate the morphine dose in mg/kg. The side labels indicate the absence (0) or presence (1) of Pgp inhibitor GF120918. The columns and rows indicated with (all) display the combination of all dose groups or all Pgp inhibitor groups, respectively.

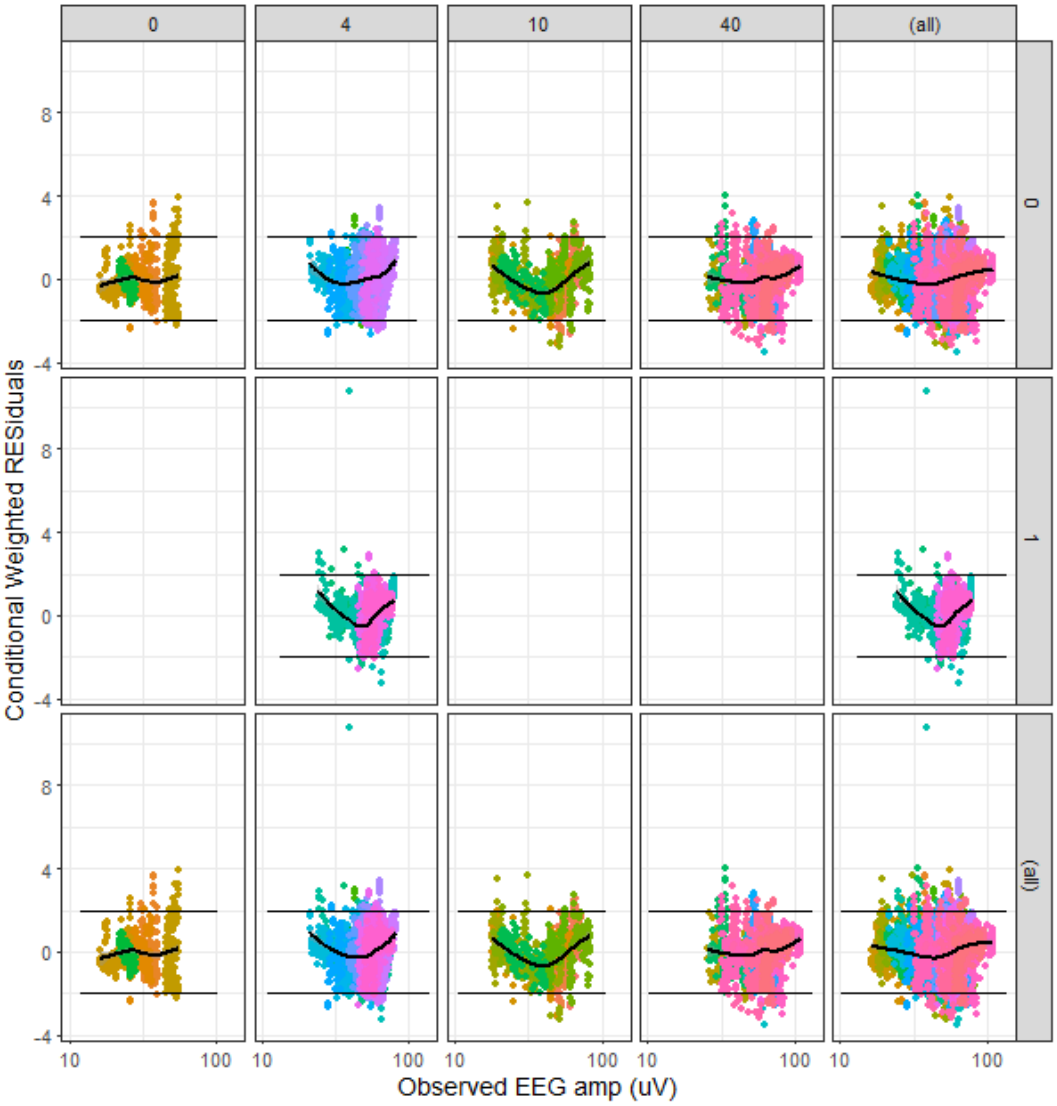

Figure S 8. Conditional weighted residuals versus observed EEG amplitudes. for the different dose groups and dose group combinations in the model fit of $EC_{PL}1$. The top labels indicate the morphine dose in mg/kg. The side labels indicate the absence (0) or presence (1) of Pgp inhibitor GF120918. The columns and row indicated with (all) display the combination of all dose groups or all Pgp inhibitor groups, respectively.

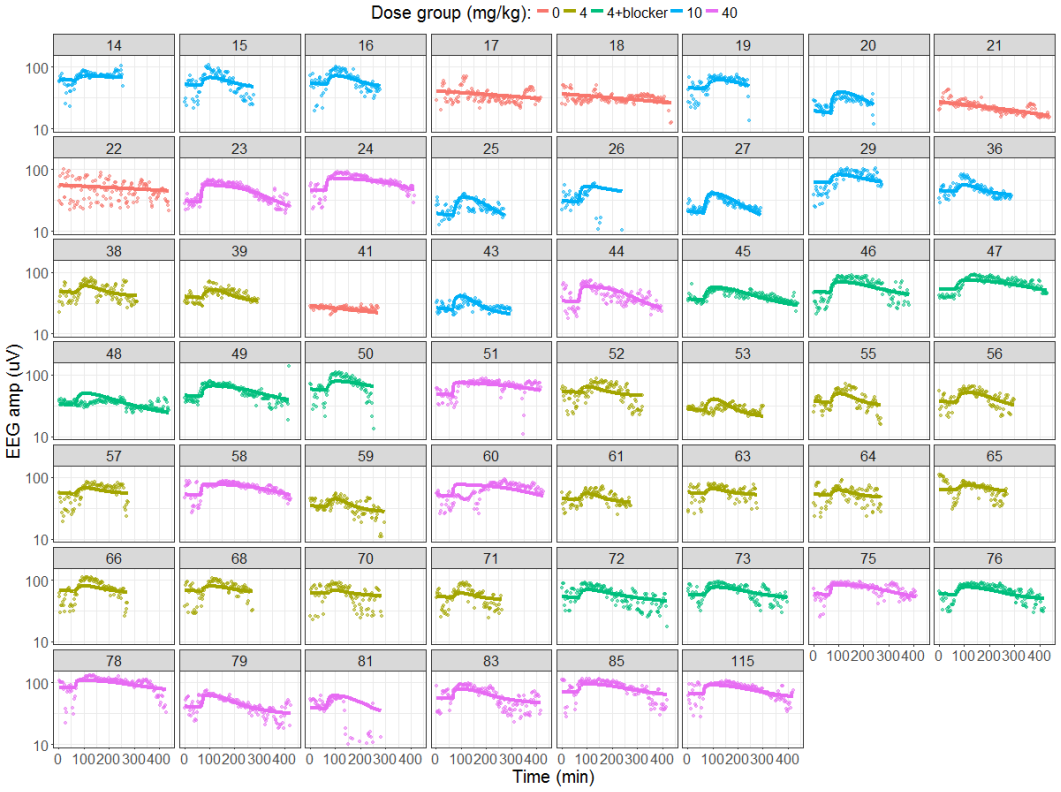

Figure S 9. Individual model fits of model $EC_{PL}1$ to the EEG data. The colors represent the different dose groups. Dots represent the observations, lines the model predictions.

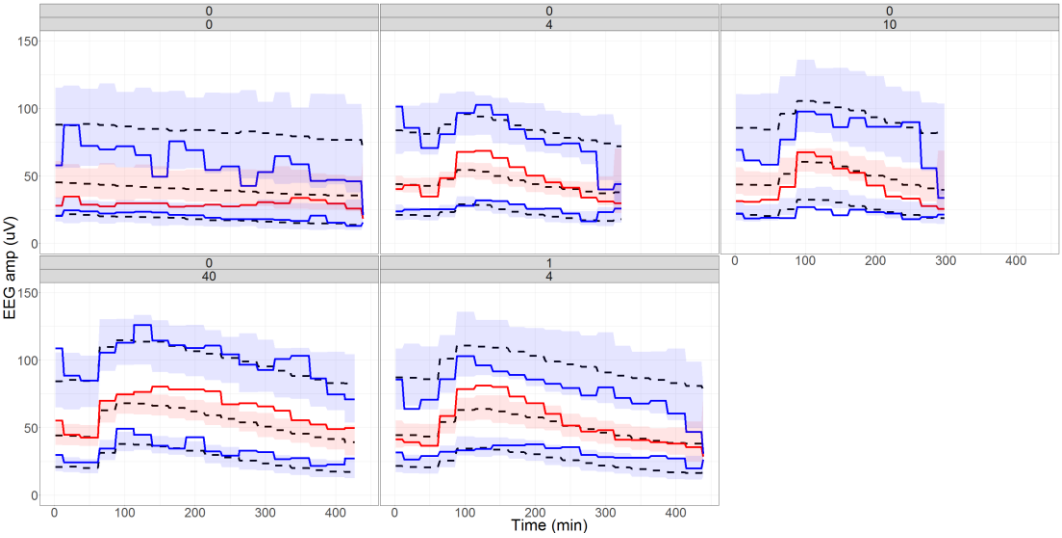

Figure S 10. Visual predictive check of the model fit of model $EC_{PL}1$. The upper labels indicate the absence (0) or presence (1) of Pgp inhibitor GF120918. The lower labels indicate the morphine dose in mg/kg. The solid lines represent the observed 5%, 50% and 95% quantiles of the data. The dashed lines represent the median of the 5%, 50% and 95% quantiles of the simulated datasets. The shaded areas represent the 5%-95% percent interval of the 5%, 50% and 95% quantiles of the simulated datasets.

Model equations and VPC for model EC-TB_{PL}1

The model equations for the EC-TB_{PL} model are provided in equations 13-15. In these equations, A_{EFF} and V_{EFF} refer to the amount and volume of the effect compartment, respectively. A_{RL} and V_{RL} refer to the amount and volume of the drug-target complex compartment, respectively. A_{Rtot} and V_{Rtot} refer to the amount and volume of the bound plus unbound target compartment, respectively. The rate constants k_{e0} and k_{off} are first order rate constants of distribution and dissociation, respectively. k_{on} is the second order association rate constant. E_0 is the baseline EEG amplitude, slope is the linear decline of the EEG amplitude per time unit, independent of the drug effect and Emax is the maximal drug effect.

13. $$\frac{d\frac{A_{EFF}}{V_{EFF}}}{dt} = k_{e0} \cdot \left(\frac{A_{EFF}}{V_{EFF}} - \frac{A_1}{V_1}\right)$$

14. $$\frac{d\frac{A_{RL}}{V_{RL}}}{dt} = k_{on} \cdot \frac{A_{EFF}}{V_{EFF}} \cdot \left(Rtot - \frac{A_{RL}}{V_{RL}}\right) - k_{off} \cdot \frac{A_{RL}}{V_{RL}}$$

15. $$Effect\,(EEG\ amplitude) = E_0 + slope * t + \frac{E_{max} \cdot \frac{A_{RL}}{V_{RL}}}{\frac{A_{Rtot}}{V_{Rtot}}}$$

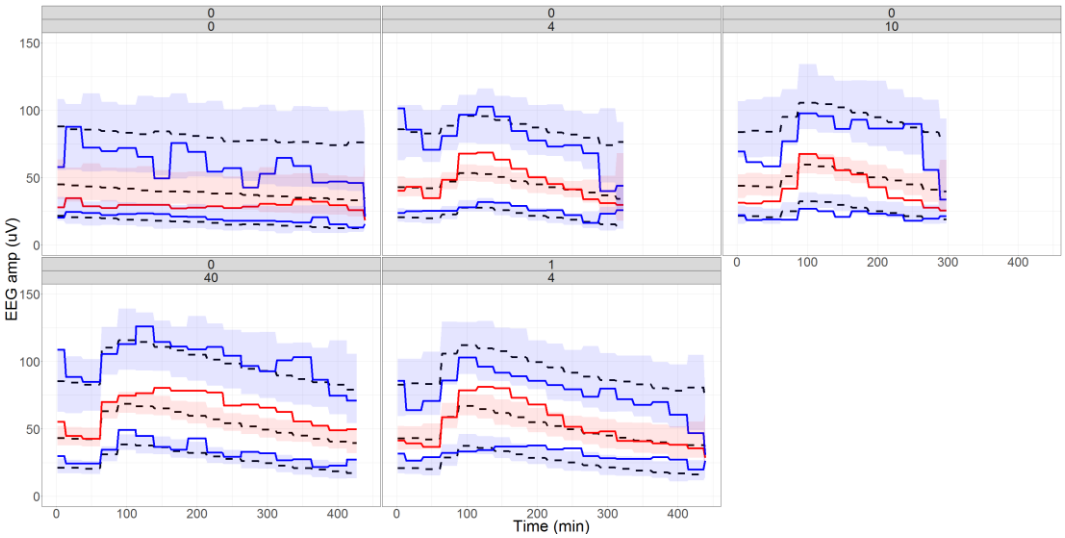

Figure S 11. Visual predictive check of the model fit of model EC-TB_{PL}1. The upper labels indicate the absence (0) or presence (1) of Pgp inhibitor GF120918. The lower labels indicate the morphine dose in mg/kg. The solid lines represent the observed 5%, 50% and 95% quantiles of the data. The dashed lines represent the median of the 5%, 50% and 95% quantiles of the simulated datasets.

Model equations and VPC for model TB_{PL}4

The model equations for the combined TB_{PL} model are provided in equations 16 and 17. In these equations, A_{RL} and V_{RL} refer to the amount and volume of the drug-target complex compartment, respectively. A_{Rtot} and V_{Rtot} refer to the amount and volume of the bound plus unbound target compartment, respectively. The rate constants k_{off} is the first order rate constants of drug-target dissociation. k_{on} is the second order association rate constant. E_0 is the baseline EEG amplitude, slope is the linear decline of the EEG amplitude per time unit, independent of the drug effect and Emax is the maximal drug effect.

16. $$\frac{d\frac{A_{RL}}{V_{RL}}}{dt} = k_{on} \cdot \frac{A_c}{V_C} \cdot \left(Rtot - \frac{A_{RL}}{V_{RL}}\right) - k_{off} \cdot \frac{A_{RL}}{V_{RL}}$$

17. $$Effect\ (EEG\ amplitude) = E_0 + slope * t + \frac{E_{max} \cdot \frac{A_{RL}}{V_{RL}}}{\frac{A_{Rtot}}{V_{Rtot}}}$$

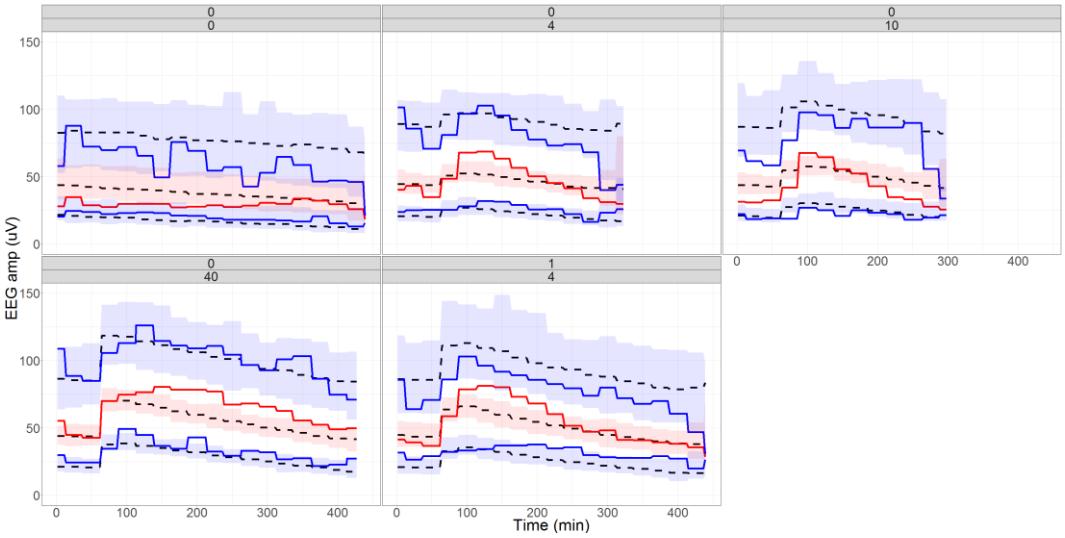

Figure S 12. Visual predictive check of the model fit of model $TB_{PL}4$. The upper labels indicate the absence (0) or presence (1) of Pgp inhibitor GF120918. The lower labels indicate the morphine dose in mg/kg. The solid lines represent the observed 5%, 50% and 95% quantiles of the data. The dashed lines represent the median of the 5%, 50% and 95% quantiles of the simulated datasets.

Supplement S 2. Dose-dependency of $Tmax_{TO}$ in a TB_{PL}.

To obtain a better understanding of the influence of dose on the $Tmax_{TO}$ in a TB_{PL} model, some of the underlying simulations for Figure 5 are shown in this section. In Figure S 13, the simulation with the lowest values of k_{on} and k_{off} is showing that in this situation, the $Tmax_{TO}$ has a high value, but also that there is no difference between the two doses. This can be understood by comparing the rate of equilibration in a situation with a constant ligand concentration with the rate of elimination.

The rate of equilibration (k_{obs}) for a constant ligand concentration [L] can be calculated by equation 1 [46]:

$k_{obs} = kon * [L] + koff$ (1)

Since the ligand concentration in our simulations is normalized for the value of K_D, equation 1 can be rewritten as equation 2, in which c is the ratio $[L]/K_D$:

$k_{obs} = kon * c * koff/kon + koff = koff*(c + 1)$ (2)

From equation 2, it can be observed that a low value of koff leads to slow equilibration, unless the ligand concentration is much higher than the affinity. If the equilibration rate is slow, the $Tmax_{TO}$ is mainly determined by the elimination rate constant, which is independent on the dose/ligand concentration. Thus, a low value of koff gives similar $Tmax_{TO}$ values for different doses, as confirmed in Figure S 13.

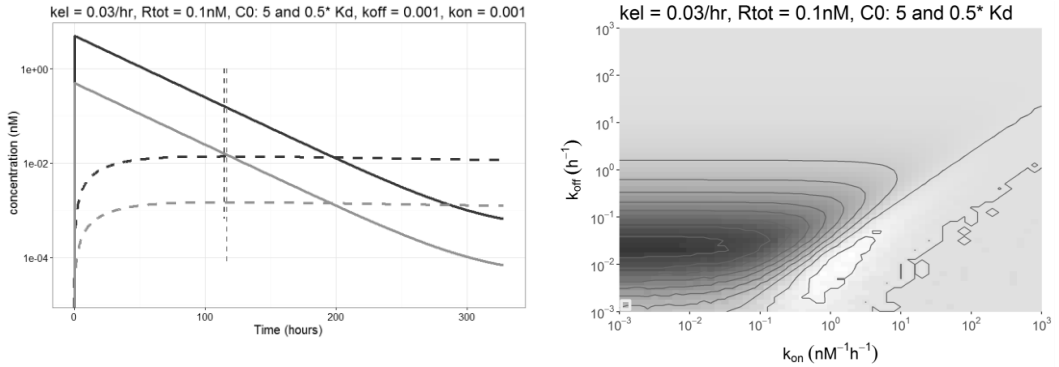

Figure S 13. Simulation of drug target binding for two different doses. The solid lines indicate plasma concentrations for the high (dark grey line) dose and the low (light grey line) dose. The dashed lines indicate target-bound drug concentrations. The vertical dotted lines indicate the time point of the maximal target-bound concentration for each dose. In this simulation, the elimination rate constant k_{el} was 0.03/hr and the target concentration was 0.1 nM. The initial concentrations for the high and the low dose corresponded to 5 and 0.5 times the K_D, respectively. The k_{on} and k_{off} values were 0.001 nM^{-1} h^{-1} and 0.001 h^{-1}, respectively, representing the area of Figure 5 that is indicated with the square in the right panel.

A high value of k_{off} gives rise to fast equilibration and a significant influence of the dose on the equilibration time, because equilibration is now much faster than elimination, and thus determining the $Tmax_{TO}$. However, because of the fast equilibration, the decrease in $Tmax_{TO}$ with increasing doses is difficult to detect because all $Tmax_{TO}$ values are low, and the absolute difference is low as well, as illustrated in Figure S 14.

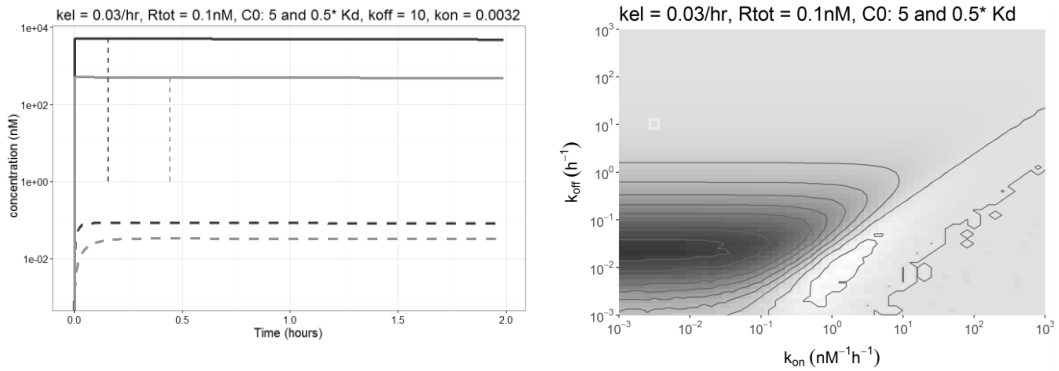

Figure S 14. Simulation of drug target binding for two different doses. The solid lines indicate plasma concentrations for the high (dark grey line) dose and the low (light grey line) dose. The dashed lines indicate target-bound drug concentrations. The vertical dotted lines indicate the time point of the maximal target-bound concentration for each dose. In this simulation, the elimination rate constant k_{el} was 0.03/hr and the target concentration was 0.1 nM. The initial concentrations for the high and the low dose corresponded to 5 and 0.5 times the K_D, respectively. The k_{on} and k_{off} values were 0.0032 nM^{-1} h^{-1} and 10 h^{-1}, respectively, representing the area of Figure 5 that is indicated with the square in the right panel.

A low value of the K_D (and therefore a low dose) will also lead to a difference in $Tmax_{TO}$ which is negligibly small or sometimes even negative (i.e. the highest dose leads to the highest $Tmax_{TO}$ value). In this area the assumption of a constant ligand concentration does not hold anymore, even when there is no elimination of the drug. This is caused by the depletion of ligand as a result of drug-target binding. When the ligand concentration is much lower than the target concentration, the equilibration rate can now be approximated by assuming the target concentration (Rtot) is constant, according to equation 3:

$$k_{obs} = kon * [Rtot] + koff \quad (3)$$

From equation 3, it should be observed that there is no influence of the ligand concentration any more, and therefore the dose does not influence the $Tmax_{TO}$ anymore. The small band in Figure 5 where the difference in $Tmax_{TO}$ values is negative can be explained by the situation where the lowest dose has the same target concentration and drug concentration. In this case, both the target and the drug concentration decline upon drug-target binding and equilibration is twice as fast compared to the situation with a constant target or ligand concentration. This can make the equilibration of the lowest dose faster than that of the highest dose. An example of such a situation is shown Figure S 15.

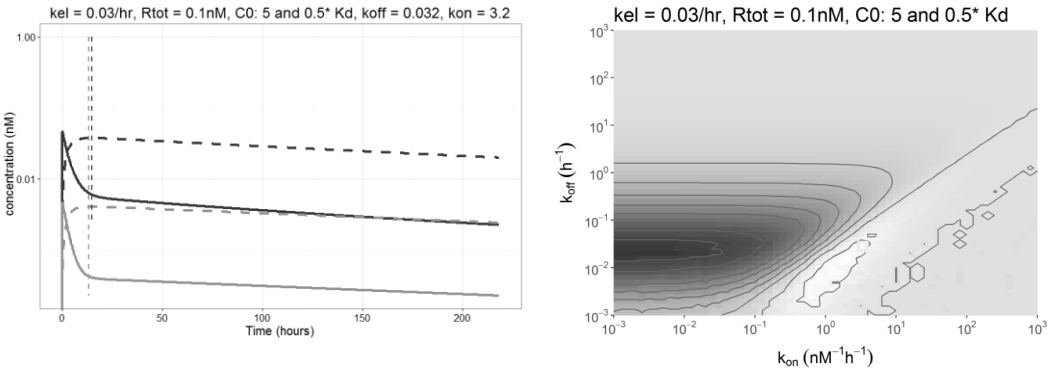

Figure S 15. Simulation of drug target binding for two different doses. The solid lines indicate plasma concentrations for the high (dark grey line) dose and the low (light grey line) dose. The dashed lines indicate target-bound drug concentrations. The vertical dotted lines indicate the time point of the maximal target-bound concentration for each dose. In this simulation, the elimination rate constant k_{el} was 0.03/hr and the target concentration was 0.1 nM. The initial concentrations for the high and the low dose corresponded to 5 and 0.5 times the K_D, respectively. The k_{on} and k_{off} values were 3.2 nM^{-1} h^{-1} and 0.032 h^{-1}, respectively, representing the area of Figure 5 that is indicated with the yellow square in the right panel.

To observe a change in $Tmax_{TO}$, it follows from the previous examples that the value of k_{off} should be low enough to make the change in $Tmax_{TO}$ observable, but it should not be so low that the elimination of the drug determines the $Tmax_{TO}$. Moreover, the initial concentration of the drug should not be lower than the target concentration. An example of such a situation is given in Figure S 16. Additionally, the lines $k_{off} = k_{el}/(c+1)$ and $K_D = Rtot/(c+1)$ align reasonably well with the middle and the diagonal end of the area where $Tmax_{TO}$ is most significant, where c represents the initial concentration/K_D ratio for the lowest dose as shown in Figure S 17.

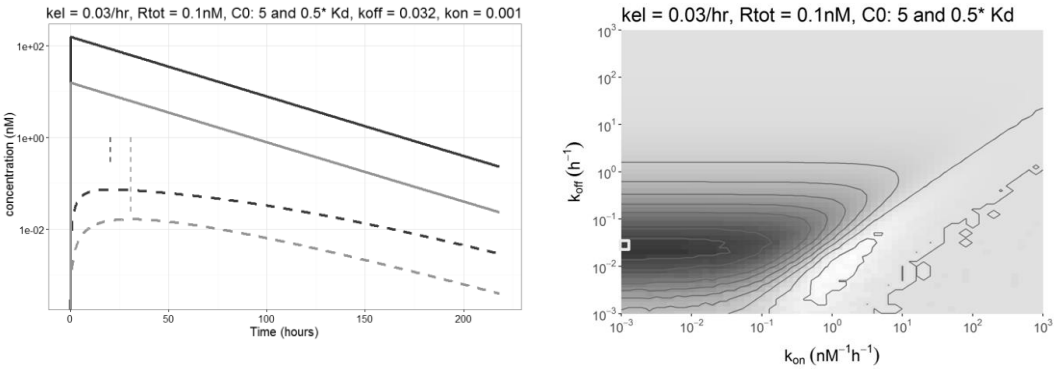

Figure S 16. Simulation of drug target binding for two different doses. The solid lines indicate plasma concentrations for the high (dark grey) dose and the low (light grey) dose. The dashed lines indicate target-bound drug concentrations. The vertical dotted lines indicate the time point of the maximal target-bound concentration for each dose. In this simulation, the elimination rate constant k_{el} was 0.03/hr and the target concentration was 0.1 nM. The initial concentrations for the high and the low dose corresponded to 5 and 0.5 times the K_D, respectively. The k_{on} and k_{off} values were 0.001 nM^{-1} h^{-1} and 0.032 h^{-1}, respectively, representing the area of Figure 5 that is indicated with the yellow square in the right panel.

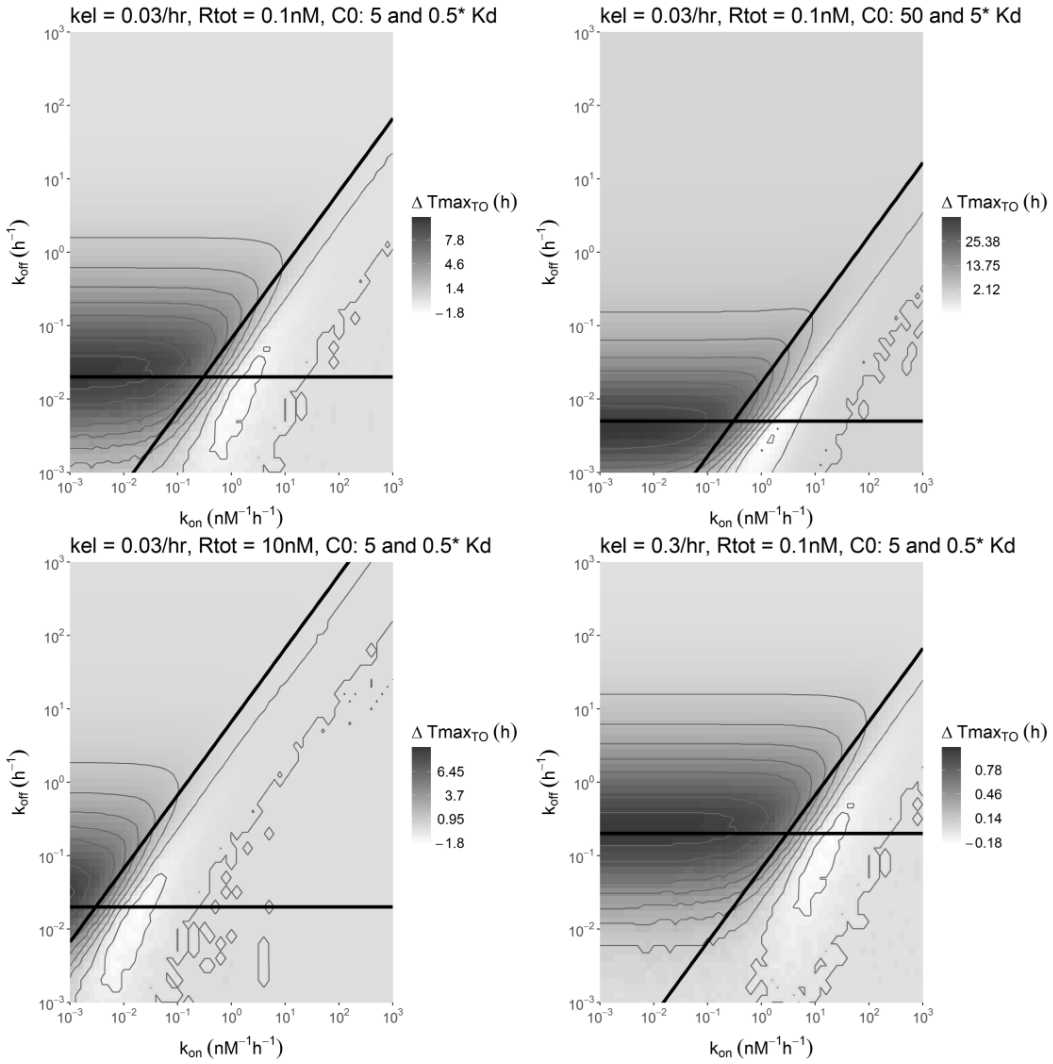

Figure S 17. Overview of the $\Delta Tmax_{TO}$ that was observed in the simulations as a result of the change in the affinity-normalized dose for different combinations of parameter values as indicated above the panels. All panels vary only one parameter compared to the upper left panel. The horizontal and diagonal lines represent the equations $k_{off} = k_{el}/(c+1)$ and $K_D = Rtot/(c+1)$, respectively, where c represents the initial concentration/K_D ratio for the lowest dose.

Supplement S 3. Asymptotic analysis of $Tmax_{TO}$ and its dependency on the dose.

1 One compartment model with drug-target binding

The model for drug-target binding is given by

$$\frac{dL}{dt} = -k_{el}L - k_{on}LR + k_{off}B$$

$$\frac{dB}{dt} = k_{on}LR - k_{off}B,$$

where

- L is the drug concentration,
- R is the **free** receptor concentration,
- B is the concentration of bound complex of L and R : $[LR]$,
- k_{on} is the rate constant at which L binds to free receptors,
- k_{off} is the rate constant at which L unbinds,
- k_{el} is the elimination rate constant.

Now, we use that the **total** receptor concentration is described by R_{tot} so that $R + B = R_{tot}$, and hence, $R = R_{tot} - B$. Then, after substituting this expression for R, the system becomes

$$\frac{dL}{dt} = -k_{el}L - k_{on}L(R_{tot} - B) + k_{off}B$$

$$\frac{dB}{dt} = k_{on}L(R_{tot} - B) - k_{off}B,$$

and hence,

$$\frac{dL}{dt} = -(k_{on}R_{tot} + k_{el})L + (k_{on}L + k_{off})B$$

$$\frac{dB}{dt} = k_{on}R_{tot}L - (k_{on}L + k_{off})B.$$

We study this system together with the initial conditions $L(0) = c\dfrac{k_{off}}{k_{on}} = cK_D$ and $B(0) = 0$.

The aim of this analysis is to determine the value of t where B attains a maximum for general c. We denote this maximum by $Tmax_{TO}(c)$. Furthermore, the interest is to determine the difference in $Tmax_{TO}(c)$ for two (different) values of c. More specifically for $c = c_1$ and $c = c_2$ where $c_2 > c_1$, we want to determine $Tmax_{TO}(c_2) - Tmax_{TO}(c_1)$.

2. Rescaling the system

In order to be able to analyse system (1.1), we rescale it by using the fact that both L and B can maximally reach certain concentrations. From the initial conditions it follows that the drug L is limited by drug dose $L(0) = cK_D = c\dfrac{k_{off}}{k_{on}}$. Also, the bound complex is limited by the total receptor concentration R_{tot}. This suggests to rescale L with cK_D and B with R_{tot}, and therefore, set $L = cK_D u$ and $B = R_{tot}v$. Then system (1.1) becomes

$$\frac{du}{dt} = -k_{el}u + k_{on}R_{tot}[-u + (u + \frac{1}{c})v]$$

$$\frac{dv}{dt} = ck_{off}[u - (u + \frac{1}{c})v],$$

with $u(0) = 1$ and $v(0) = 0$. In this system u corresponds to L and v to B.

Next, we study system (2.1) in different parameter regions and determine the value of t for which v attains a maximum.We use the different sets of coefficients present in system (2.1) to determine the various regions. In these regions, we use asymptotic analysis to determine an asymptotic expansion for v from which we determine the leading order of $Tmax_{TO}(c)$.

To define the regions, we look at the groups of parameters present in system (2.1) and set them to be equal. This gives us the following lines

$$ck_{off} = k_{el}$$

$$k_{off} = k_{el}$$

$$k_{off} = k_{on}R_{tot}$$

$$ck_{off} = \frac{k_{on}R_{tot}}{c}$$

$$k_{on}R_{tot} = k_{el}$$

$$k_{on}R_{tot} = ck_{el}.$$

In the following analysis, we assume that c is of order 1, hence $c = O(1)$, then we define various regions

$$I.\quad ck_{off} = O(k_{el}) \text{ and } R_{tot} << K_D$$

$$II.\quad k_{el} << k_{off} \text{ and } R_{tot} << K_D$$

$$III.\quad k_{off} << k_{el} \text{ and } R_{tot} << K_D$$

$$IV.\quad k_{el} << k_{off} \text{ and } R_{tot} >> K_D$$

$$V.\quad k_{off} << k_{el} \text{ and } R_{tot} >> K_D.$$

Note that since $c = O(1)$, not all the lines in (2.2) are needed when defining these regions. On the other hand, when *c* >> 1, the different lines are essential.

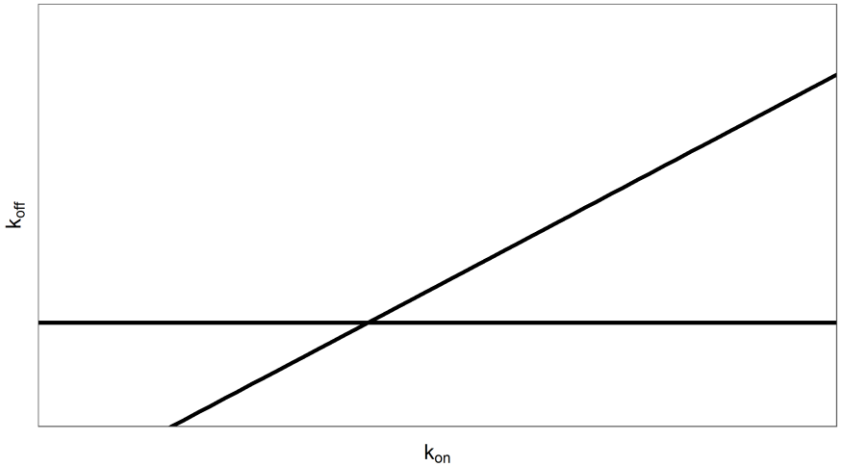

Figure S18: Sketch of the different regions in the (k_{on}, k_{off}) *-plane and the lines* $k_{off} = k_{el}$ *and* $R_{tot} = K_D$ *for* $c > 1$.

In these regions, we can find an asymptotic expression for v and determine the leading order expression for $Tmax_{TO}$. Here, we summarise the results.

In region I , we find that $Tmax_{TO}$ must satisfy an implicit relation depending on the different parameters. We introduce $a = \frac{ck_{off}}{k_{el}} = \mathrm{O}(1)$ then $Tmax_{TO} = \frac{\tau}{k_{el}}$, where τ must satisfy

$$a(c + e^{\tau}) e^{a(ce^{-\tau} - \tau)} \int_0^{\tau} e^{-ace^{-s} + (a-1)s} ds = 1.$$

In the other regions we can determine the leading order of $Tmax_{TO}$ explicitly, this yields:

$$II. \quad Tmax_{TO} = -\frac{1}{(c+1)k_{off}} \log\left(\frac{k_{el}}{(c+1)^2 k_{off}}\right)$$

$$III. \quad Tmax_{TO} = -\frac{1}{k_{el}} \log\left(\frac{k_{off}}{k_{el}}\right)$$

$$IV.\quad Tmax_{TO} = -\frac{1}{k_{on}R_{tot}}\log\left((c+1)\frac{k_{off}}{k_{on}R_{tot}}\right)$$

$$V.\quad Tmax_{TO} = \frac{1}{k_{el}}.$$

Note that we denote with log the natural logarithm, $\ln$.

Hence, we find that when $k_{off} << k_{el}$ (in regions III and V) that $Tmax_{TO}$ **does not depend on** c, and therefore, is independent of the dosis, to leading order. For $k_{off} >> k_{el}$ (in regions II and IV), we find from the above expressions that $Tmax_{TO}$ **is small**, and so the dependence on the dose does also not play a role.

Note that the above results are not true for $c >> 1$. We briefly study that case in section 5.

To show how we obtain the above results, we give the details of the asymptotic analysis in two of the regions in the next sections.

3. The analysis in region III

We choose the parameters to lie in region III such that $R_{tot} << K_D$ and $k_{off} << k_{el}$. Then, we rescale time as $\tau = k_{el}t$ in this region and system (2.1) becomes

$$\frac{du}{d\tau} = -u + \delta[-u + (u + \frac{1}{c})v]$$

$$\frac{dv}{d\tau} = \varepsilon[u - (u + \frac{1}{c})v].$$

where $\delta = \frac{k_{on}R_{tot}}{k_{el}}$ and $\varepsilon = \frac{ck_{off}}{k_{el}}$. From the choice of the relation between the parameters, we find that $\delta << \varepsilon << 1$. Now, we assume the following asymptotic expansions for u and v

$$u = u_0 + \varepsilon u_{10} + \delta u_{01} + \text{higher order terms},$$

$$v = v_0 + \varepsilon v_{10} + \delta v_{01} + \text{higher order terms}.$$

And, from the initial conditions for system (2.1), it follows that $u_0(0)=1, u_{ij}(0)=0$, $v_{ij}(0)=0$ for all i, j.

In the following we assume that δ and ε^2 are not of the same order. Next, we substitute the above expansions into system (3.1), collect terms at different orders and solve the corresponding equations at each level.

At $O(1)$, we find that

$$\frac{du_0}{d\tau} = -u_0$$

$$\frac{dv_0}{d\tau} = 0.$$

This can be solved and, together with the initial conditions, this leads to $v_0 = 0$ and $u_0 = e^{-\tau}$.

Next, at $O(\varepsilon)$ we obtain

$$\frac{du_{10}}{d\tau} = -u_{10}$$

$$\frac{dv_{10}}{d\tau} = u_0 - (u_0 + \frac{1}{c})v_0 = u_0.$$

Together with the initial conditions, this gives $u_{10} = 0$ and $v_{10} = 1 - e^{-\tau}$. Since this v_{10} does not attain a maximum, we need to determine higher order terms in the expansion of v.

Then, at $O(\delta)$ we find

$$\frac{du_{01}}{d\tau} = -u_{01} - u_0 + (u_0 + \frac{1}{c})v_0$$

$$\frac{dv_{01}}{d\tau} = 0,$$

which yields $v_{01} = 0$. It turns out we don't need u_{01} to determine $Tmax_{TO}$ so we refrain from giving that here.

At $O(\varepsilon^2)$ we obtain

$$\frac{dv_{20}}{d\tau} = u_{10} - (u_0 + \frac{1}{c})v_{10} - u_{10}v_0$$

$$= -(e^{-\tau} + \frac{1}{c})(1 - e^{-\tau})$$

$$= e^{-2\tau} + \frac{1-c}{c}e^{-\tau} - \frac{1}{c}.$$

From this, we find

$$v_{20} = \frac{1}{2}(1 - e^{-2\tau}) - \frac{\tau}{c} + \frac{1-c}{c}(1 - e^{-\tau}).$$

Since we do not need u_{20} for further analysis, we also do not give that here.

Now, collecting the various terms, we find that

$$v(\tau) = \varepsilon(1 - e^{-\tau}) + \varepsilon^2\left(\frac{1}{2}(1 - e^{-2\tau}) + \frac{1-c}{c}(1 - e^{-\tau}) - \frac{\tau}{c}\right)$$

to leading order. Using this expression, we can obtain a leading order expression for $Tmax_{TO}$. Differentiating we find

$$\frac{dv}{d\tau} = \varepsilon e^{-\tau} + \varepsilon^2\left(e^{-2\tau} + \frac{1-c}{c}e^{-\tau} - \frac{1}{c}\right).$$

Setting this expression to zero, we can find $Tmax_{TO}$ from a balance between the first and the last term. Hence, we set $\varepsilon e^{-\tau} = \varepsilon^2 \frac{1}{c}$ which leads to

$$\tau = -\log(\frac{\varepsilon}{c}).$$

Rescaling back to original variables and parameters, we obtain

$$Tmax_{TO} = -\frac{1}{k_{el}} \log(\frac{k_{off}}{k_{el}}).$$

4. The analysis in region V

In this section, we choose the parameters to lie in region V such that $k_{off} << k_{el}$ and $K_D << R_{tot}$. We rescale time as $\tau = k_{on} R_{tot} t$ in this region and system (2.1) becomes

$$\frac{du}{d\tau} = -\delta u - u + (u + \frac{1}{c})v$$

$$\frac{dv}{d\tau} = \varepsilon[u - (u + \frac{1}{c})v],$$

where $\delta = \frac{k_{el}}{k_{on} R_{tot}}$ and $\varepsilon = \frac{c k_{off}}{k_{on} R_{tot}}$. From the choice of the relation between the parameters, we find that $\varepsilon << \delta << 1$. Now, we assume the following asymptotic expansions for u and v

$$u = u_0 + \delta u_{01} + \varepsilon u_{10} + \textit{higher order terms},$$

$$v = v_0 + \delta v_{01} + \varepsilon v_{10} + \textit{higher order terms}.$$

From the initial conditions for system (2.1), it follows that $u_0(0) = 1, u_{ij}(0) = 0$, $v_{ij}(0) = 0$ for all i, j.

In the following we assume that δ^2 and ε are not of the same order. Next, we substitute the above expansions into system (4.1), collect terms at different orders and solve the corresponding equations at each level.

At $O(1)$ we find that

$$\frac{du_0}{d\tau} = -u_0 + (u_0 + \frac{1}{c})v_0$$

$$\frac{dv_0}{d\tau} = 0.$$

This can be solved and, together with the initial conditions, this leads to $v_0 = 0$ and $u_0 = e^{-\tau}$.

Next, at $O(\delta)$ we find

$$\frac{du_{01}}{d\tau} = -u_{01} - u_0 + (u_0 + \frac{1}{c})v_{01}$$

$$\frac{dv_{01}}{d\tau} = 0,$$

which yields $v_{01} = 0$. Solving for u_{01} leads to

$$u_{01} = -\tau e^{-\tau}.$$

At $O(\varepsilon)$ we obtain

$$\frac{du_{10}}{d\tau} = -u_{10} + (u_0 + \frac{1}{c})v_{10} + u_{10}v_0$$

$$\frac{dv_{10}}{d\tau} = u_0 - (u_0 + \frac{1}{c})v_0 = u_0.$$

Together with the initial conditions, this gives $v_{10} = 1 - e^{-\tau}$. We do not give u_{10} since we will not need it in the further analysis. Again, v_{10} does not attain maximum, and therefore, we need higher order terms in the expansion of v.

At $O(\delta^2)$ we find that $v_{02} = 0$ and so we need to go to $O(\varepsilon\delta)$ where

$$\frac{dv_{11}}{d\tau} = u_{01} - (u_0 + \frac{1}{c})v_{01} - u_{10}v_0$$

$$= -\tau e^{-\tau}.$$

Hence,

$$v_{11} = (\tau + 1)e^{-\tau} - 1,$$

and the expansion for v reads

$$v = \varepsilon\left(1 - e^{-\tau} + \delta((\tau+1)e^{-\tau} - 1)\right),$$

to leading order. Differentiating leads to

$$\frac{dv}{d\tau} = \varepsilon\left(e^{-\tau} - \delta\tau e^{-\tau}\right),$$

which becomes zero when

$$\tau = \frac{1}{\delta}.$$

Rescaling back to original variables and parameters, we obtain

$$Tmax_{TO} = \frac{1}{\delta k_{on} R_{tot}} = \frac{1}{k_{el}}.$$

5. The case when $c >> 1$.

Next, we briefly look at the case when $c >> 1$. Then, the results are different from before. One essential difference is that the regions now depend on c where $c >> 1$.

We will only give results for region I. Note that this region shifts down in the (k_{on}, k_{off}) -plane compared to before.

We do still find that $Tmax_{TO}$ must satisfy an implicit relation depending on the different parameters. We find that $Tmax_{TO} = \frac{\tau}{k_{el}}$, where τ must satisfy

$$e^{a(e^{-\tau}-1)-\tau} - \frac{1}{c}\left(1 - e^{a(e^{-\tau}-1)} + ae^{ae^{-\tau}-\tau}(\tau e^{-b} - \int_0^\tau e^{-ae^{-s}} ds)\right) = 0,$$

and $a = \frac{ck_{off}}{k_{el}} = \mathrm{O}(1)$.